IOP Publishing
Reports on Progress in Physics
Rep. Prog. Phys. **81** (2018) 016901 (33pp)
https://doi.org/10.1088/1361-6633/aa997e

Review

Dark energy two decades after: observables, probes, consistency tests

Dragan Huterer[1] **and Daniel L Shafer**[2]

[1] Department of Physics, University of Michigan, 450 Church Street, Ann Arbor, MI 48109, United States of America
[2] Department of Physics and Astronomy, Johns Hopkins University, 3400 North Charles Street, Baltimore, MD 21218, United States of America

E-mail: huterer@umich.edu and dshafer2@jhu.edu

Received 12 October 2016, revised 19 September 2017
Accepted for publication 9 November 2017
Published 12 December 2017

Corresponding Editor Professor Leszek Roszkowski

Abstract
The discovery of the accelerating universe in the late 1990s was a watershed moment in modern cosmology, as it indicated the presence of a fundamentally new, dominant contribution to the energy budget of the universe. Evidence for dark energy, the new component that causes the acceleration, has since become extremely strong, owing to an impressive variety of increasingly precise measurements of the expansion history and the growth of structure in the universe. Still, one of the central challenges of modern cosmology is to shed light on the physical mechanism behind the accelerating universe. In this review, we briefly summarize the developments that led to the discovery of dark energy. Next, we discuss the parametric descriptions of dark energy and the cosmological tests that allow us to better understand its nature. We then review the cosmological probes of dark energy. For each probe, we briefly discuss the physics behind it and its prospects for measuring dark energy properties. We end with a summary of the current status of dark energy research.

Keywords: dark energy, observational cosmology, large-scale structure

(Some figures may appear in colour only in the online journal)

1. Introduction

The discovery of the accelerating universe in the late 1990s [1, 2] was a watershed moment in modern cosmology. It unambiguously indicated the presence of a qualitatively new component in the universe, one that dominates the energy density today, or of a modification of the laws of gravity. Dark energy quickly became a centerpiece of the new standard cosmological model, which also features baryonic matter, dark matter, and radiation (photons and relativistic neutrinos). Dark energy naturally resolved some tensions in cosmological parameter measurements of the 1980s and early 1990s, explaining in particular the fact that the geometry of the universe was consistent with the flatness predicted by inflation, while the matter density was apparently much less than the critical value necessary to close the universe.

The simplest and best-known candidate for dark energy is the energy of the vacuum, represented in Einstein's equations by the cosmological-constant term. Vacuum energy density, unchanging in time and spatially smooth, is currently in good agreement with existing data. Yet, there exists a rich set of other dark energy models, including evolving scalar fields, modifications to general relativity, and other physically-motivated possibilities. This has spawned an active research area focused on describing and modeling dark energy and its effects on the expansion rate and the growth of density fluctuations, and this remains a vibrant area of cosmology today.

Over the past two decades, cosmologists have been investigating how best to measure the properties of dark energy. They have studied exactly what each cosmological probe can say about this new component, devised novel cosmological tests for the purpose, and planned observational surveys with the principal goal of precision dark energy measurements. Both ground-based and space-based surveys have been planned, and there are even ideas for laboratory tests of the physical phenomena that play a role in some dark energy models. Current measurements have already sharply improved constraints on dark energy; as a simple example, the statistical evidence for its existence, assuming a cosmological constant but not a flat universe, is nominally over 66σ[3]. Future observations are expected to do much better still, especially for models that allow a time-evolving dark energy equation of state. They will allow us to map the expansion and growth history of the universe at the percent level, beginning deep in the matter-dominated era, into the period when dark energy dominates, and up to the present day.

Despite the tremendous observational progress in measuring dark energy properties, no fundamentally new insights into the physics behind this mysterious component have resulted. Remarkably, while the error bars have shrunk dramatically, current constraints are still roughly consistent with the specific model that was originally quoted as the best fit in the late 1990s—a component contributing about 70% to the current energy budget with an equation-of-state ratio $w \simeq -1$. This has led some in the particle physics and cosmology community to suspect that dark energy really is just the cosmological constant Λ and that its unnaturally-small value is the product of a multiverse, such as would arise from the framework of eternal inflation or from the landscape picture of string theory, which generically features an enormous number of vacua, each with a different value for Λ. In this picture, we live in a vacuum which is able to support stars, galaxies, and life, making our tiny Λ a necessity rather than an accident or a signature of new physics. As such reasoning may be untestable and therefore arguably unscientific, many remain hopeful that cosmic acceleration can be explained by testable physical theory that does not invoke the anthropic principle. For now, improved measurements provide by far the best opportunity to better understand the physics behind the accelerating universe.

Figure 1 shows the energy density of species in the universe as a function of $(1+z)$, which is equivalent to the inverse of the scale factor a. The dashed vertical line indicates the present time ($z = 0$), with the past to the left and the future to the right. Notice that radiation, which scales as $(1+z)^4$, dominates the early universe. Matter scales as $(1+z)^3$ and overtakes radiation at $z \simeq 3400$, corresponding to $t \simeq 50\,000$ yr after the big bang. Dark energy shows a very different behavior; vacuum energy density is precisely constant in time, and even dynamical dark energy, when constrained to fit current data, allows only a modest variation in density with time. The shaded region in figure 1 indicates the region allowed at 1σ (68.3% confidence) by combined constraints from current data (see figure 9) assuming the equation of state is allowed to vary as $w(a) = w_0 + w_a\,(1-a)$.

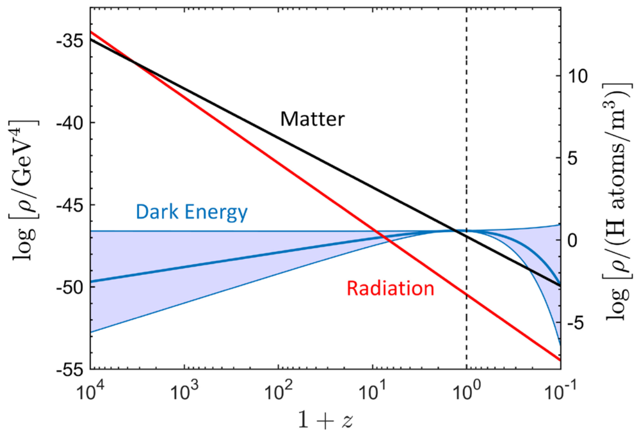

Figure 1. Energy density of species in the universe as a function of $(1+z)$, where z is the redshift. The dashed vertical line indicates the present time ($z = 0$), with the past to the left and future to the right. Note that matter ($\propto (1+z)^3$) and radiation ($\propto (1+z)^4$) energy densities scale much faster with the expanding universe than the dark energy density, which is exactly constant for a cosmological constant Λ. The shaded region for dark energy indicates the energy densities allowed at 1σ (68.3% confidence) by combined constraints from current data assuming the equation of state is allowed to vary as $w(z) = w_0 + w_a\,z/(1+z)$.

Our goal is to broadly review cosmic acceleration for physicists and astronomers who have a basic familiarity with cosmology but may not be experts in the field. This review complements other excellent, and often more specialized, reviews of the subject that focus on dark energy theory [5–7], cosmology [8], the physics of cosmic acceleration [9], probes of dark energy [10, 11], dark energy reconstruction [12], dynamics of dark energy models [13], the cosmological constant [14, 15], and dark energy aimed at astronomers [16]. A parallel review of dark energy theory is presented in this volume by Brax.

The rest of this review is organized as follows. In section 2, we provide a brief history of the discovery of dark energy and how it changed our understanding of the universe. In section 3, we outline the mathematical formalism that underpins modern cosmology. In section 4, we review empirical parametrizations of dark energy and other ways to quantify our constraints on geometry and growth of structure, as well as modified gravity descriptions. We review the principal cosmological probes of dark energy in section 5 and discuss complementary probes in section 6. In section 7, we summarize key points regarding the observational progress on dark energy.

2. The road to dark energy

In the early 1980s, inflationary theory shook the world of cosmology by explaining several long-standing conundrums [17–19]. The principal inflationary feature is a mechanism to accelerate the expansion rate so that the universe appears

[3] To obtain this number, we maximized the likelihood over all parameters, first with the dark energy density a free parameter and then with it fixed to zero, using the same current data as in figure 9. We quote the number of standard deviations of a (one-dimensional) Gaussian distribution corresponding to this likelihood ratio.

precisely flat at late times. As one of inflation's cornerstone predictions, flatness became the favored possibility among cosmologists. At the same time, various direct measurements of mass in the universe were typically producing answers that were far short of the amount necessary to close the universe.

Notably, the baryon-to-matter ratio measured in galaxy clusters, combined with the baryon density inferred from big bang nucleosynthesis, effectively ruled out the flat, matter-dominated universe, implying instead a low matter density $\Omega_m \sim 0.3$ [20–22]. Around the same time, measurements of galaxy clustering—both the amplitude and shape of the correlation function—indicated strong preference for a low-matter-density universe and further pointed to the concordance cosmology with the cosmological constant contributing to make the spatial geometry flat [23, 24]. The relatively high values of the measured Hubble constant at the time ($H_0 \simeq 80$ km/s/Mpc [25]), combined with the lower limit on the age of the universe inferred from the ages of globular clusters ($t_0 > 11.2$ Gyr at 95% confidence [26]), also disfavored a high-matter-density universe. Finally, the discovery of massive clusters of galaxies at high redshift $z \sim 1$ [27, 28] independently created trouble for the flat, matter-dominated universe.

While generally in agreement with measurements, such a low-density universe *still* conflicted with the ages of globular clusters, even setting aside inflationary prejudice for a flat universe. Also, the results were not unambiguous: throughout the 1980s and early 1990s, there was claimed evidence for a much higher matter density from measurements of galaxy fluxes [31] and peculiar velocities (e.g. [32–34]), along with theoretical forays that have since been disfavored, such as inflation models that result in an open universe [35, 36] and extremely low values of the Hubble constant [37]. Even the early type Ia supernova studies yielded inconclusive results [38].

Attempts to square the theoretical preference for a flat universe with uncertain measurements of the matter density included a proposal for the existence of a nonzero cosmological constant Λ. This term, corresponding to the energy density of the vacuum, would need to have a tiny value by particle physics standards in order to be comparable to the energy density of matter today. Once considered by Einstein to be the mechanism that guarantees a static universe [39], it was soon disfavored when it became clear that such a static universe is unstable to small perturbations, and it was abandoned once it became established that the universe is actually expanding. Entertained as a possibility in 1980s [40, 41], the cosmological constant was back in full force in the 1990s [24, 42–48]. Nevertheless, it was far from clear that anything other than matter, plus a small amount of radiation, comprises the energy density in the universe today.

A breakthrough came in late 1990s. Two teams of supernova observers, the Supernova Cosmology Project (led by Saul Perlmutter) and the High-Z Supernova Search Team (led by Brian Schmidt) developed an efficient approach to use the world's most powerful telescopes working in concert to discover and follow up supernovae. These teams identified procedures to guarantee finding batches of SNe in each run (for a popular review of this, see [49]).

Another breakthrough came in 1993 by Mark Phillips, an astronomer working in Chile [3]. He noticed that the SN Ia luminosity (or absolute magnitude) is correlated with the decay time of the SN light curve. Phillips considered the quantity Δm_{15}, the decay of the light from the SN 15 days after the maximum. He found that Δm_{15} is strongly correlated with the SN intrinsic brightness (estimated using other methods). The *Phillips relation* (left panel of figure 2) is roughly the statement that 'broader is brighter'. That is, SNe with broader light curves tend to have a larger intrinsic luminosity. This broadness can be quantified by a 'stretch factor' that scales the width of the light curve [2]. By applying a correction based on stretch (right panel of figure 2), astronomers found that the intrinsic dispersion of the SN Ia luminosity, initially ~0.3–0.5 mag, can be reduced to ~0.2 mag after correction for stretch. Note that this corresponds to an error in distance of $\delta d_L/d_L = [\ln(10)/5]\,\delta m \sim 10\%$. The Phillips relation was the second key ingredient that enabled SNe Ia to achieve the precision needed to reliably probe the contents of the universe.

A third important ingredient was the ability to separate intrinsic variation in individual SN luminosities from extinction due to intervening dust along the line of sight, which leads to reddening. This separation requires SN Ia color measurements, achieved by observing and fitting SN Ia light curves in multiple wavebands (e.g. [50]).

The final, though chronologically the first, key step for the discovery of dark energy was the development and application of charge-coupled devices (CCDs) in observational astronomy, and they equipped cameras of increasingly large size [51–57].

Some of the early SN Ia results came in the period 1995–1997 but were based on only a few high-redshift SNe and therefore had large uncertainties (e.g. [38]).

2.1. The discovery of dark energy

The definitive results, based on 16 [1] and 42 [2] high-redshift supernovae, followed soon thereafter. The results of the two teams agreed and indicated that the distant SNe are dimmer than would be expected in a matter-only universe. In other words, they were farther away than expected, suggesting that the expansion rate of the universe is increasing, contrary to the expectation for a matter-dominated universe with *any* amount of matter. Over the following decade, larger and better SN samples [58–62] confirmed and strengthened the original findings, while discoveries of very-high-redshift ($z > 1$) objects played an important role by providing evidence for the expected earlier epoch of deceleration [63–65].

This accelerated expansion of the universe requires the presence of a new component with strongly negative pressure. To see this, consider the *acceleration equation*, which governs the behavior of an expanding universe (see section 3 for a more complete introduction to basic cosmology):

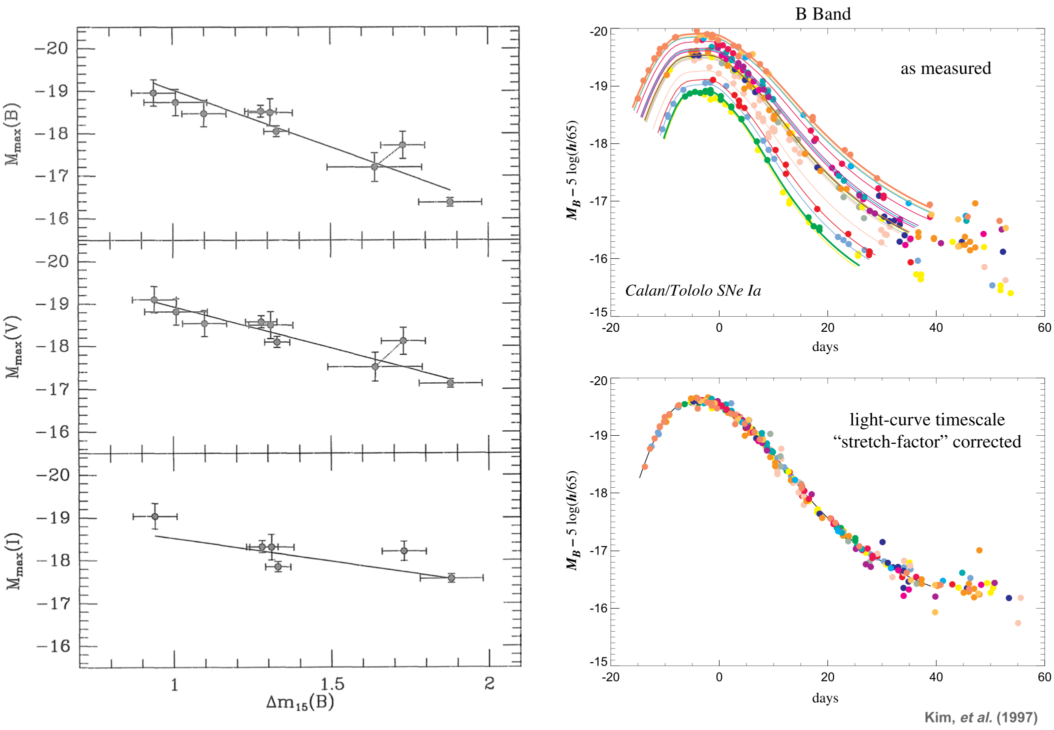

Figure 2. Key properties of type Ia supernovae that enabled them to become a powerful tool to discover the acceleration of the universe. *Left panel*: The Phillips relation, reproduced from his 1993 paper [3]. © IOP Publishing Ltd. All rights reserved. The (apparent) magnitude of SNe Ia is correlated with Δm_{15}, the decay of the light curve 15 days after the maximum. *Right panel*: Light curves for a sample of SNe Ia before (top) and after (bottom) correction for stretch (essentially, the Phillips relation); reproduced with permission from [4].

$$\frac{\ddot{a}}{a} = -\frac{4\pi G}{3}\,(\rho + 3p) = -\frac{4\pi G}{3}\,(\rho_m + \rho_{\rm de} + 3p_{\rm de})\,,$$

where ρ and p are the energy density and pressure of all components in the universe, including matter and a new component we call dark energy (radiation contributes negligibly at redshifts much less than $\sim$1000, and the pressure of cold dark matter can also be ignored). Accelerated expansion of the universe is equivalent to $\ddot{a} > 0$, and this can happen only when the pressure of the new component is strongly negative. In terms of the dark energy equation of state $w \equiv p_{\rm de}/\rho_{\rm de}$, acceleration only occurs when $w < -1/3\,(1 + \rho_m/\rho_{\rm de})$; therefore, regardless of matter density, acceleration never occurs when $w > -1/3$.

Stronger evidence for dark energy has followed in parallel with drastically improved constraints on other cosmological parameters, particularly by the cosmic microwave background (CMB) anisotropy measurements and measurements of the baryon acoustic oscillation (BAO) feature in the clustering of galaxies (both of which will be discussed at length in section 5). In figure 3, we show the Hubble diagram (plot of magnitude versus redshift) for modern SN Ia data from the ‘Supercal’ compilation [29], binned in redshift, along with recent BAO measurements that also measure distance versus redshift [30], and finally the theory expectation for the currently favored Λ-cold-dark-matter (ΛCDM) model, a Λ-only model, and matter-only models without dark energy spanning the open, closed, and flat geometry. In figure 4, we show the evolution of constraints in the plane of matter density relative to critical Ω_m and dark energy equation of state w, beginning around the time of dark energy discovery (circa 1998), then about a decade later (circa 2008), and finally in the present day (circa 2016), nearly two decades later.

The discovery of the accelerating universe via SN Ia observations was a dramatic event that, almost overnight, overturned the previously favored matter-only universe and pointed to a new cosmological standard model dominated by a negative-pressure component. This component that causes the expansion of the universe to accelerate was soon named ‘dark energy’ by cosmologist Michael Turner [66]. The physical nature of dark energy is currently unknown, and the search for it is the subject of worldwide research that encompasses theory, observation, and perhaps even laboratory experiments. The physics behind dark energy has connections to fundamental physics, to astrophysical observations, and to the ultimate fate of the universe.

3. Modern cosmology: the basics

We will begin with a brief overview of the physical foundations of modern cosmology.

The cosmological principle states that, on large enough scales, the universe is homogeneous (the same everywhere) and isotropic (no special direction). It is an assumption but also a testable hypothesis, and indeed there is excellent observational evidence that the universe satisfies the cosmological principle on its largest spatial scales (e.g. [67, 68]). Under these assumptions, the metric can be written in the Robertson-Walker (RW) form

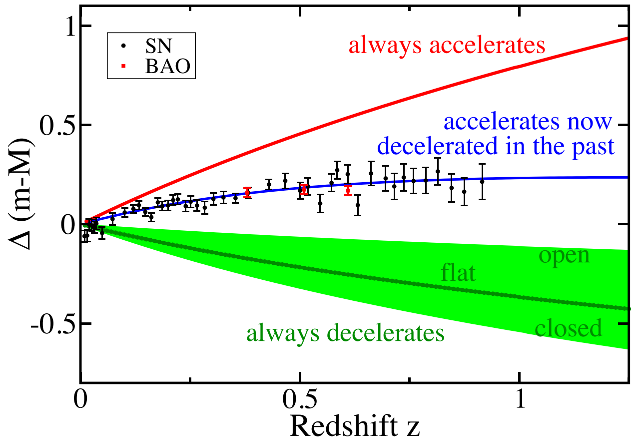

Figure 3. Evidence for the transition from deceleration in the past to acceleration today. The blue line indicates a model that fits the data well; it features acceleration at relatively late epochs in the history of the universe, beginning a few billion years ago but still billions of years after the big bang. For comparison, we also show a range of matter-only models in green, corresponding to $0.3 \leqslant \Omega_m \leqslant 1.5$ and thus spanning the open, flat, and closed geometries without dark energy. Finally, the red curve indicates a model that *always* exhibits acceleration and that also does not fit the data. The black data points are binned distance moduli from the Supercal compilation [29] of 870 SNe, while the three red data points represent the distances inferred from the most recent BAO measurements (BOSS DR12 [30]).

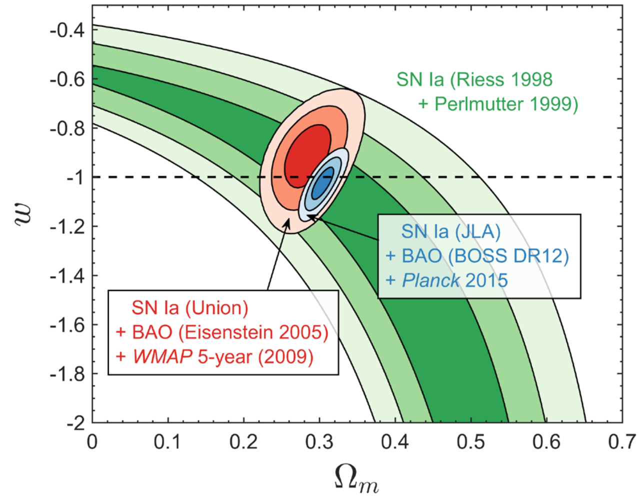

Figure 4. History of constraints on key dark energy parameters Ω_m and a constant equation of state w, assuming a flat universe such that $\Omega_{\rm de} = 1 - \Omega_m$. The three sets of contours show the status of measurements around the time of dark energy discovery (circa 1998; green), roughly a decade later following precise measurements of CMB anisotropies and the detection of the BAO feature (circa 2008; red), and in the present day, nearly two decades after discovery (circa 2016; blue). Note that, to estimate the 1998 constraints, we analyze a combined set of SNe from the two independent analyses, discarding duplicates but first comparing the very similar low-redshift samples to infer the (arbitrary) magnitude offset between the two.

$$ds^2 = dt^2 - a^2(t)\left[\frac{dr^2}{1-kr^2} + r^2\left(d\theta^2 + \sin^2\theta\, d\phi^2\right)\right],$$

where r, θ, and ϕ are comoving spatial coordinates, t is time, and the expansion is described by the cosmic scale factor $a(t)$, where the present value is $a(t_0) = 1$ by convention. The quantity k is the intrinsic curvature of three-dimensional space; $k = 0$ corresponds to a spatially flat universe with Euclidean geometry, while $k > 0$ corresponds to positive curvature (spherical geometry) and $k < 0$ to negative curvature (hyperbolic geometry).

The scale factor $a(t)$ is a function of the energy densities and pressures of the components that fill the universe. Its evolution is governed by the Friedmann equations, which are derived from Einstein's equations of general relativity using the RW metric:

$$H^2 \equiv \left(\frac{\dot a}{a}\right)^2 = \frac{8\pi G\rho}{3} - \frac{k}{a^2} + \frac{\Lambda}{3}, \qquad (1)$$

$$\frac{\ddot a}{a} = -\frac{4\pi G}{3}(\rho + 3p) + \frac{\Lambda}{3}, \qquad (2)$$

where H is the Hubble parameter, Λ is the cosmological constant term, ρ is the total energy density, and p is the pressure. Note that the cosmological constant Λ can be subsumed into the energy density ρ, but separating out Λ reflects how it was incorporated historically, before the discovery of the accelerating universe.

We can define the critical density $\rho_{\rm crit} \equiv 3H^2/(8\pi G)$ as the density that leads to a flat universe with $k = 0$. Then the effect of dark energy on the expansion rate can be described by its present-day energy density relative to critical $\Omega_{\rm de}$ and its equation of state w, which is the ratio of pressure to energy density:

$$\Omega_{\rm de} \equiv \frac{\rho_{\rm de,0}}{\rho_{\rm crit,0}}; \qquad w \equiv \frac{p_{\rm de}}{\rho_{\rm de}}. \qquad (3)$$

The simplest possibility is that the equation of state is constant in time. This is in fact the case for (cold, nonrelativistic) matter ($w_{\rm matter} = 0$) and radiation ($w_{\rm rad} = 1/3$). However, it is also possible that w evolves with time (or redshift). The continuity equation,

$$\dot\rho = -3H(\rho + p), \qquad (4)$$

is not an independent result but can be derived from (1) and (2). An expression of conservation of energy, it can used to solve for the dark energy density as a function of redshift for an arbitrary equation of state $w(z)$:

$$\begin{aligned}\rho_{\rm de}(z) &= \rho_{\rm de,0}\,\exp\left[3\int_0^z \frac{1+w(z')}{1+z'}dz'\right] \\ &= \rho_{\rm de,0}\,(1+z)^{3(1+w)},\end{aligned} \qquad (5)$$

where the second equality is the simplified result for constant w.

The expansion rate of the universe $H \equiv \dot a/a$ from (1) can then be written as (again for $w =$ constant)

$$\begin{aligned}H^2 = H_0^2\,&\left[\Omega_m(1+z)^3 + \Omega_r(1+z)^4\right. \\ &\left.+\,\Omega_{\rm de}(1+z)^{3(1+w)} + \Omega_k(1+z)^2\right],\end{aligned} \qquad (6)$$

where H_0 is the present value of the Hubble parameter (the Hubble constant), Ω_m and Ω_r are the matter and radiation energy densities relative to critical, and the dimensionless curvature 'energy density' Ω_k is defined such that $\sum_i \Omega_i = 1$. Since $\Omega_r \simeq 8 \times 10^{-5}$, we can typically ignore the radiation contribution for low-redshift ($z \lesssim 10$) measurements; however, near the epoch of recombination ($z \sim 1000$), radiation contributes significantly, and at earlier times ($z \gtrsim 3300$), it dominates.

3.1. Distances and geometry

Observational cosmology is complicated by the fact that we live in an expanding universe where distances must be defined carefully. Astronomical observations, including those that provide clues about nature of dark energy, fundamentally rely on two basic techniques, measuring fluxes from objects and measuring angles on the sky. It is therefore useful to define two types of distance, the luminosity distance and the angular diameter distance. The luminosity distance d_L is the distance at which an object with a certain luminosity produces a certain flux ($f = L/(4\pi d_L^2)$), while the angular diameter distance d_{A} is the distance at which a certain (transverse) physical separation x_{trans} produces a certain angle on the sky ($\theta = x_{\mathrm{trans}}/d_{\mathrm{A}}$). For a (homogeneous and isotropic) Friedmann–Robertson–Walker universe, the two are closely related and given in terms of the comoving distance $r(z)$:

$$d_L(z) = (1+z)\, r(z); \qquad d_{\mathrm{A}}(z) = \frac{1}{1+z}\, r(z)\,. \tag{7}$$

The comoving distance can be written compactly as

$$r(z) = \lim_{\Omega_k' \to \Omega_k} \frac{c}{H_0\sqrt{\Omega_k'}} \sinh\left[\sqrt{\Omega_k'} \int_0^z \frac{H_0}{H(z')}\,\mathrm{d}z'\right], \tag{8}$$

which is valid for all Ω_k (positive, negative, zero) and where $H(z)$ is the Hubble parameter (e.g. (6)).

Having specified the effect of dark energy on the expansion rate and the distances, its effect on any quantity that fundamentally only depends on the expansion rate can be computed. For example, number counts of galaxy clusters are sensitive to the volume element of the universe, given by

$$\frac{\mathrm{d}V}{\mathrm{d}z\,\mathrm{d}\Omega} = \frac{r^2(z)}{H(z)/c},$$

where $\mathrm{d}z$ and $\mathrm{d}\Omega$ are the redshift and solid angle intervals, respectively. Similarly, some methods rely on measuring ages of galaxies, which requires knowledge of the age-redshift relation. The age of the universe for an arbitrary scale factor $a = 1/(1+z)$ is given by

$$t(a) = \int_0^a \frac{\mathrm{d}a'}{a' H(a')}\,.$$

We will make one final point here. Notice from (8) that, when calculating distance, the dark energy parameters Ω_{de} and w are hidden behind an integral (and behind *two* integrals when a general $w(z)$ is considered; see (5)). The Hubble parameter $H(z)$ is in the integrand of the distance formula and therefore requires one fewer integral to calculate; it depends more directly on the dark energy parameters. Therefore, direct measurements of the Hubble parameter, or of quantities that depend directly on $H(z)$, are nominally more sensitive to dark energy than observables that fundamentally depend on distance. Unfortunately, measurements of $H(z)$ are more difficult to achieve and/or are inferred somewhat indirectly, such as from differential distance measurements.

3.2. Density fluctuations

Next we turn to the growth of matter density fluctuations, $\delta \equiv \delta\rho_m/\rho_m$. Assuming that general relativity holds, and assuming small matter density fluctuations $|\delta| \ll 1$ on length scales much smaller than the Hubble radius, the temporal evolution of the fluctuations is given by

$$\ddot{\delta}_k + 2H\dot{\delta}_k - 4\pi G\rho_{\mathrm{m}}\delta_k = 0, \tag{9}$$

where δ_k is the Fourier component[4] corresponding to the mode with wavenumber $k \simeq 2\pi/\lambda$. In (9), dark energy enters twofold: in the friction term, where it affects H; and in the source term, where it reduces ρ_{m}. For $H(z)$ normalized at high redshift, dark energy increases the expansion rate at $z \lesssim 1$, stunting the growth of density fluctuations.

The effect of dark energy on growth is illustrated in the top right panel of figure 5, where we show the growth-suppression factor $g(z)$, which indicates the amount of growth relative to that in an Einstein-de Sitter universe, which contains no dark energy. It is implicitly defined with respect to the scaled linear growth of fluctuations,

$$D(a) \equiv \frac{\delta(a)}{\delta(1)} \equiv \frac{a\,g(a)}{g(1)}. \tag{10}$$

With only matter, $D(a) = a$ and $g(a) = 1$ at all times. In the presence of dark energy, $g(a)$ falls below unity at late times. In the currently favored ΛCDM model, $g(1) \simeq 0.78$. The value of the density fluctuation δ at scale factor a, relative to the matter-only case, is suppressed by a factor $g(a)$, while the two-point correlation function is suppressed by g^2.

A useful alternative expression for the growth suppression is

$$g(a) = \exp\left[\int_0^a \frac{\mathrm{d}a'}{a'}\,(f(a') - 1)\right], \tag{11}$$

where

$$f(a) \equiv \frac{\mathrm{d}\ln D}{\mathrm{d}\ln a} \approx \Omega_m(a)^\gamma \tag{12}$$

is the growth rate which, as we will see below, contains very important sensitivity to both dark energy parameters and to modifications to gravity. The latter, approximate equality in (12) is remarkably accurate provided $\gamma \simeq 0.55$. While this functional form for $f(a)$ had been noted long, in the context of the matter-only universe, before the discovery of dark energy [69], the formula remains percent-level accurate even for a wide variety of dark energy models with varying equations of

[4] Given our assumptions, each wavenumber evolves independently, though this does not always hold for modified theories of gravity, even in linear theory.

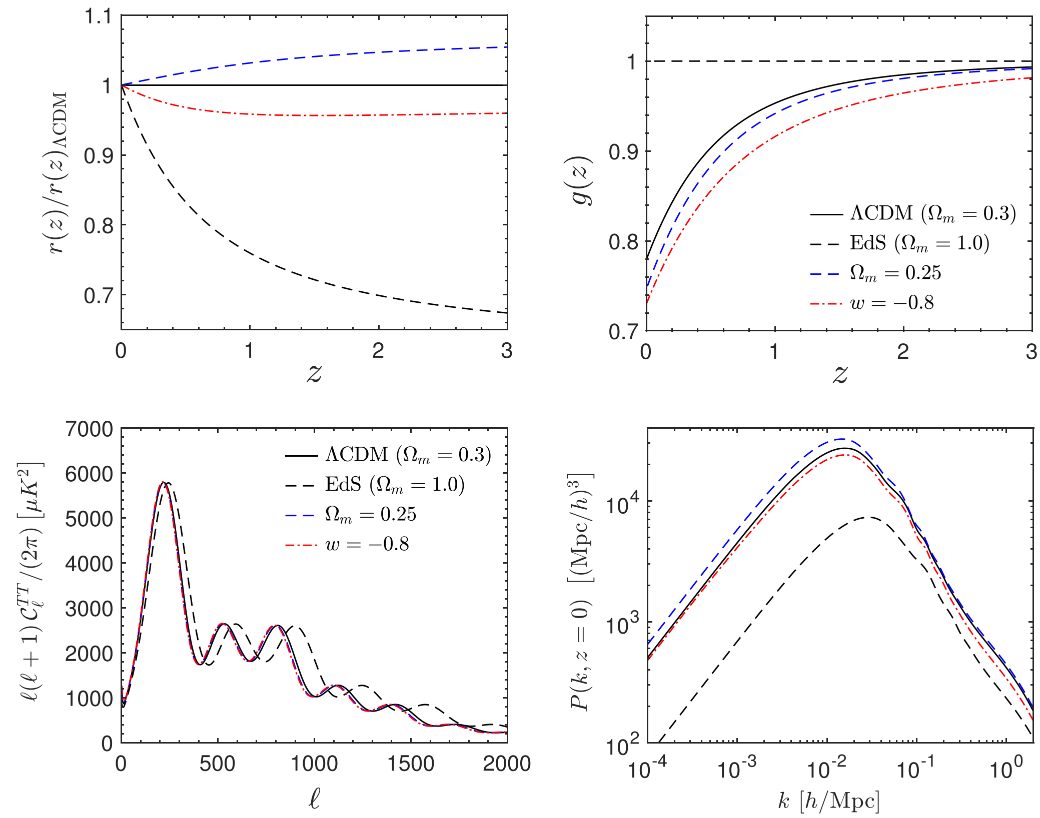

Figure 5. Dependence of key cosmological observables on dark energy. The top left and right panels show, respectively, the comoving distance (8) and growth suppression (relative to the matter-only case) from (10). The bottom left and right panels show, respectively, the CMB angular power spectrum $\mathcal{C}_\ell$ as a function of multipole ℓ and the matter power spectrum $P(k)$ as a function of wavenumber k. For each observable, we indicate the prediction for a fiducial ΛCDM model ($\Omega_m = 0.3$, $w = -1$) and then illustrate the effect of varying the indicated parameter. In each case, we assume a flat universe and hold the combination $\Omega_m h^2$ fixed.

state as long as we set $\gamma = 0.55 + 0.05[1 + w(z = 1)]$ [70, 71].

The two point function is often phrased in terms of the Fourier transform of the configuration-space two-point function—the matter power spectrum, defined via

$$\langle \delta_{\vec{k}}\, \delta^*_{\vec{k}'} \rangle = (2\pi)^3\, \delta^{(3)}(\vec{k} - \vec{k}')\, P(k) \tag{13}$$

where we note that $P(\vec{k}) = P(k)$ due to homogeneity. We can write the general formula for the power spectrum of density fluctuations in the dimensionless form $\Delta^2(k) \equiv k^3 P(k)/(2\pi^2)$ as

$$\Delta^2(k, a) = A\, \frac{4}{25}\, \frac{1}{\Omega_m^2} \left(\frac{k}{k_{\mathrm{piv}}}\right)^{n-1} \left(\frac{k}{H_0}\right)^4 \times [ag(a)]^2\, T^2(k)\, T_{\mathrm{nl}}(k)\,, \tag{14}$$

where A is the normalization of the power spectrum (current constraints favor $A \approx 2.2 \times 10^{-9}$), k_{piv} is the 'pivot' wavenumber around which we compute the spectral index n[5], and $[ag(a)]$ is the linear growth of perturbations. $T(k)$ is the transfer function, which is constant for modes that entered the horizon before the matter-radiation equality (comoving wavenumber $k \lesssim 0.01\ h\ \mathrm{Mpc}^{-1}$) and scales as k^{-2} at smaller scales that entered the horizon during radiation domination. Finally, T_{nl} indicates a prescription for the *nonlinear* power spectrum, which is usually calibrated from N-body simulations. Recent analytic fitting formulae for this term were given in [72, 73].

[5] The *Planck* analysis uses $k_{\mathrm{piv}} = 0.05\ h\,\mathrm{Mpc}^{-1}$, where h is the dimensionless Hubble constant ($H_0 = 100h$ km/s/Mpc), but beware that $k_{\mathrm{piv}} = 0.002\ \mathrm{Mpc}^{-1}$ is occasionally used.

Finally, we outline the principal statistic that describes the distribution of hot and cold spots in the cosmic microwave background anisotropies. The angular power spectrum of the CMB anisotropies is essentially a projection along the line of sight of the primordial matter power spectrum. Adopting the expansion of the temperature anisotropies on the sky in terms of the complex coefficients $a_{\ell m}$,

$$\frac{\delta T}{T}(\hat{\boldsymbol{n}}) = \sum_{\ell=2}^{\infty} \sum_{m=-\ell}^{\ell} a_{\ell m}\, Y_{\ell m}(\hat{\boldsymbol{n}})\,, \tag{15}$$

we can obtain the ensemble average of the two point correlation function of the coefficients $C_\ell \equiv \langle |a_{\ell m}|^2 \rangle$ as

$$C_\ell = 4\pi \int \Delta^2(k)\, j_\ell^2(kr_*)\, \mathrm{d}\ln k\,,$$

where j_ℓ is the spherical bessel function and r_* is the radius of the sphere onto which we are projecting (the comoving distance to recombination); in the standard model, $r_* \simeq 14.4$ Gpc. Physical structures that appear at angular separations θ roughly correspond to power at multipole $\ell \simeq \pi/\theta$.

Basic observables and their variation when a few basic parameters governing dark energy are varied are shown in figure 5. To illustrate the effects of variations in the dark energy model, we compare the following four models:

(i) Flat model with matter density $\Omega_m = 0.3$, equation of state $w = -1$, and other parameters in agreement with the most recent cosmological constraints [74].
(ii) Same as (i), but with $\Omega_m = 1$. This is the Einstein-de Sitter model, flat and matter dominated with no dark energy. We hold all other parameters, including the combination $\Omega_m h^2$, fixed to their best-fit values in (i).
(iii) Same as (i), except $\Omega_m = 0.25$.
(iv) Same as (i), but with $w = -0.8$.

4. Parametrizations of dark energy

4.1. Introduction

Given the lack of a consensus model for cosmic acceleration, it is a challenge to provide a simple yet unbiased and sufficiently general description of dark energy. The equation-of-state parameter w has traditionally been identified as one useful phenomenological description; being the ratio of pressure to energy density, it is also closely connected to the underlying physics. Many more general parametrizations exist, some of them with appealing statistical properties. We now review a variety of formalisms that have been used to describe and constrain dark energy.

We first describe parametrizations used to describe the effects of dark energy on observable quantities. We then discuss the reconstruction of the dark-energy history; the principal-component description of it; the figures of merit; and descriptions of more general possibilities beyond spatially smooth dark energy, including modified gravity models. We end by outlining two strategies to test the internal consistency of the currently favored ΛCDM model.

4.2. Parametrizations

Assuming that dark energy is spatially smooth, its simplest parametrization is in terms of its equation-of-state [75, 76]

$$w \equiv \frac{p_{\rm de}}{\rho_{\rm de}} = \text{constant}. \tag{16}$$

This form describes vacuum energy ($w = -1$) and topological defects ($w = -N/3$, where N is the integer dimension of the defect and takes the value 0, 1, or 2 for monopoles, cosmic strings, or textures, respectively). Together with $\Omega_{\rm de}$, w provides a two-parameter description of the dark-energy sector. However, it does not describe models which have a time-varying w, such as scalar field dark energy or modified gravity, although cosmological observables are often sufficiently accurately described by a constant w even for models with mildly varying $w(z)$.

Promoting either the dark energy density or the equation of state to a general function of redshift—$\Omega_{\rm de}(z)$ or $w(z)$—would be the most general way to describe dark energy, still assuming its spatial homogeneity. In practice, however, either of these functions formally corresponds to infinitely many parameters to measure, and measuring even a few such parameters is a challenge. Perhaps not surprisingly, therefore, the most popular parametrizations of w have involved two free parameters. One of the earliest and simplest such parametrizations is linear evolution in redshift, $w(z) = w_0 + w'z$ [77]. Other low-dimensional parametrizations have been proposed [78]; for low redshift they are all essentially equivalent, but for large z they lead to different and often unphysical behavior. The parametrization [79, 80]

$$w(a) = w_0 + w_a(1-a) = w_0 + w_a\,\frac{z}{1+z}, \tag{17}$$

where $a = 1/(1+z)$ is the scale factor, avoids this problem, and it fits many scalar field and some modified gravity expansion histories. This therefore leads to the most commonly used description of dark energy, namely the three-parameter set $\{\Omega_{\rm de}, w_0, w_a\}$. The energy density is then

$$\frac{\rho_{\rm de}(a)}{\rho_{\rm crit,0}} = \Omega_{\rm de}\, a^{-3(1+w_0+w_a)} {\rm e}^{-3w_a(1-a)}. \tag{18}$$

Constraints on $w(z)$ derived from individual, marginalized constraints on w_0 and w_a are shown in the left panel of figure 8.

More general expressions have been proposed (e.g. [81, 82]); however, introducing additional parameters makes the equation of state very difficult to measure, and such extra parameters are often ad hoc and unmotivated from either a theoretical or empirical point of view.

4.3. Pivot redshift

Two-parameter descriptions of $w(z)$ that are linear in the parameters entail the existence of a ‘pivot’ redshift z_p at which the measurements of the two parameters (e.g. w_0 and w_a) are uncorrelated and the error in $w_p \equiv w(z_p)$ is minimized. Essentially, z_p indicates the redshift at which the error on $w(z)$ is tightest, for fixed assumptions about the data. This is illustrated in the left panel of figure 6. Writing the equation of state in (17) in the form

$$w(a) = w_p + (a_p - a)w_a, \tag{19}$$

it is easy to translate constraints from the (w_0, w_a) to (w_p, w_a) parametrization, as well as determine a_p (or z_p), for any particular data set. In particular, if $\mathbf{C}$ is the 2×2 covariance matrix for $\{w_0, w_a\}$ (other parameters marginalzied over), then the pivot redshift is given by [84]

$$z_p = -\frac{C_{w_0 w_a}}{C_{w_0 w_a} + C_{w_a w_a}}, \tag{20}$$

while the variance at the pivot is given by

$$\sigma^2(w_p) = C_{w_0 w_0} - \frac{C^2_{w_0 w_a}}{C_{w_a w_a}}. \tag{21}$$

Measurements of the equation of state at the pivot point often provides the most useful information in ruling out models (e.g. ruling out $w = -1$). Note that the pivot redshift (and all associated quantities, such as $\sigma(w_p)$) depend on the choice of cosmological probes and the specific data set used, therefore describing the quantities that are best measured by that data.

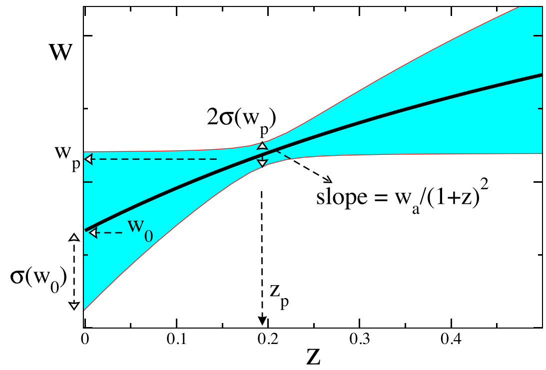

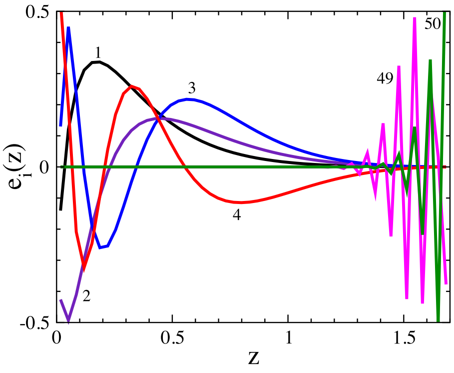

Figure 6. *Left panel*: Illustration of the main features of the popular parametrization of the equation of state [79, 80] given by $w(z) = w_0 + w_a z/(1+z)$. We indicate the pivot redshift z_p, the corresponding value of the equation of state w_p, the intercept w_0, the slope (proportional to w_a), and a visual interpretation of the approximate uncertainties in w_0 and w_p. *Right panel*: The four best-determined (labeled 1–4) and two worst-determined (labeled 49-50) principal components of $w(z)$ for a future SN Ia survey with several thousand SNe in the redshift range $0 < z < 1.7$; reprinted figure with permission from [83], Copyright (2003) by the American Physical Society.

4.4. Principal components

The cosmological function that we would like to determine—$w(z)$, $\rho_{\rm de}(z)$, or $H(z)$—can be expanded in terms of principal components, a set of functions that are uncorrelated and orthogonal by construction [83]. In this approach, the data determine which parameters are measured best.

Suppose we parametrize $w(z)$ in terms of piecewise constant values w_i $(i = 1, \dots, N)$, each defined over a narrow redshift range $z_i < z < z_i + \Delta z)$. In the limit of small Δz this recovers the shape of an arbitrary dark energy history (in practice, $N \gtrsim 20$ is sufficient [86]), but the estimates of the w_i from a given dark energy probe will be very noisy. Principal component analysis (PCA) extracts from those noisy estimates the best-measured features of $w(z)$. One finds the eigenvectors $e_i(z)$ of the inverse covariance matrix for the parameters w_i and the corresponding eigenvalues λ_i. The equation-of-state parameter is then expressed as

$$1 + w(z) = \sum_{i=1}^{N} \alpha_i\, e_i(z), \tag{22}$$

where the $e_i(z)$ are the principal components. The coefficients α_i, which can be computed via the orthonormality condition $\alpha_i = \int (1 + w(z)) e_i(z) {\rm d}z$, are each determined with an accuracy $1/\sqrt{\lambda_i}$. Several of these components are shown for a future SN survey in the right panel of figure 6, while measurements of the first ten PCs of the equation of state from recent data are shown in figure 7.

There are multiple advantages to the PC approach for dark energy (when measuring either the equation of state $w(z)$ or $\rho_{\rm de}(z)$ or $H(z)$). First, the method is as close to model-independent as one can realistically get, as no information about the temporal dependence of these functions has been assumed *a priori*[6]. In essence, we are asking the data to tell us what we measure and how well we measure it; there are no arbitrary parametrizations imposed. Second, one can use this approach to optimize survey design—for example, design a survey that is most sensitive to the dark energy equation of state parameter in some specific redshift interval. Finally, PCs make it straightforward to quantify how many independent parameters can be measured by a given combination of cosmological probes (e.g. for how many PCs is σ_{α_i} or $\sigma_{\alpha_i}/\alpha_i$ less than some threshold value [87]).

There are a variety of extensions of the PCA method, including measurements of the uncorrelated equation-of-state parameters [88] or other quantities such as the linear growth of density fluctuations [89] that also have the feature of being localized in redshift intervals, or generalizing principal components to functions in both redshift z and wavenumber k [90, 91]. The right panel of figure 8 shows constraints on four uncorrelated bins of $w(z)$ from an analysis that combines CMB, BAO, SN Ia, and Hubble constant measurements [92].

4.5. Direct reconstruction

It is tempting to consider the possibility that measurements of the comoving distance to a range of redshifts, such as those from SNe Ia, can be used to invert (8) and (5) and obtain either $\rho_{\rm de}(z)$ or $w(z)$ in full generality, without using any parametrization. This program goes under the name of direct reconstruction [66, 93–95]. The inversion is indeed analytic and the equation of state, for example, is given in terms of the first and second derivatives of the comoving distance as

$$1 + w(z) = \frac{1+z}{3}\,\frac{3H_0^2\Omega_m(1+z)^2 + 2({\rm d}^2r/{\rm d}z^2)({\rm d}r/{\rm d}z)^{-3}}{H_0^2\,\Omega_m(1+z)^3 - ({\rm d}r/{\rm d}z)^{-2}}\,. \tag{23}$$

Assuming that dark energy is due to a single rolling scalar field, the scalar potential $V(\phi)$ can also be reconstructed.

$$V\left[\phi(z)\right] = \frac{1}{8\pi G}\left[\frac{3}{({\rm d}r/{\rm d}z)^2} + (1+z)\frac{{\rm d}^2r/{\rm d}z^2}{({\rm d}r/{\rm d}z)^3}\right] - \frac{3\Omega_m H_0^2(1+z)^3}{16\pi G}\,. \tag{24}$$

One can also reconstruct the dark energy density [96, 97], which depends only on the first derivative of distance with respect to redshift,

[6] Of course, one still typically makes implicit assumptions about the speed of sound of dark energy, anisotropic stresses, etc, so the method is not truly model-independent.

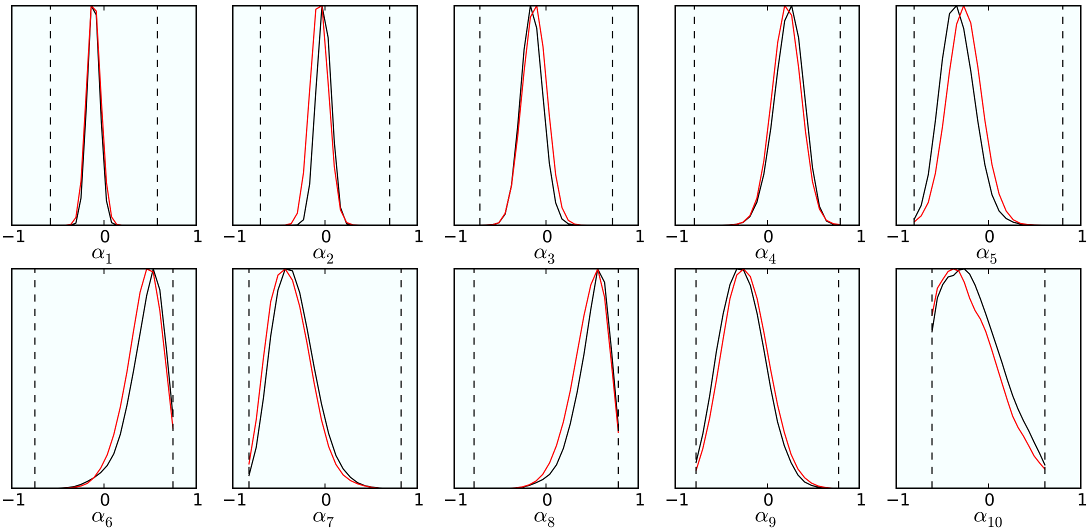

Figure 7. Marginalized posterior likelihoods for the first 10 principal components of the dark energy equation of state, based on recent (2012) data (SN Ia + BAO + CMB) and reprinted figure with permission from [85], Copyright (2012) by the American Physical Society. The dashed vertical lines represent the hard prior limits. Black curves indicate constraints when considering only the uncorrelated, statistical SN Ia uncertainties, while red curves correspond to an analysis using the full SN Ia covariance matrix, including all systematic uncertainties.

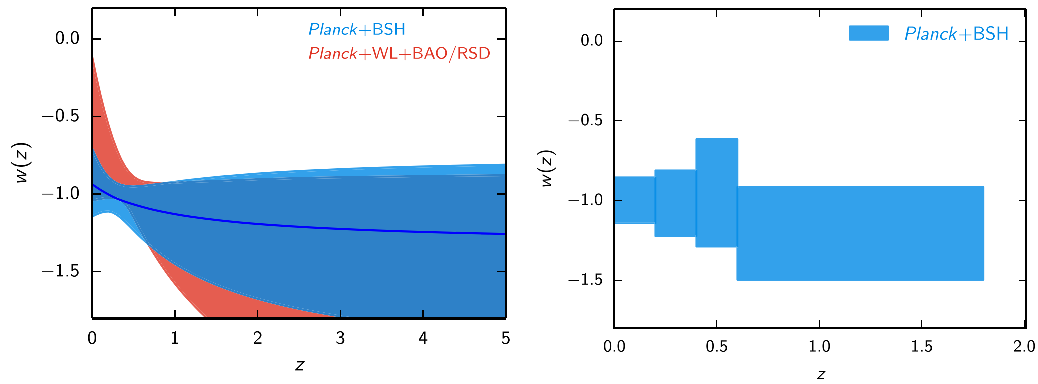

Figure 8. Constraints on the redshift evolution of the dark energy equation of state, reproduced from the *Planck* 2015 analysis [92]. *Left panel*: Constraints on $w(z)$ assuming the parametrization $w(a) = w_0 + w_a(1 - a)$. The blue curve represents the best-fit model, and the shaded regions indicate models allowed at 95% confidence level. *Right panel*: Constraints on four uncorrelated bins of $w(z)$, using the formalism of [88]. The shaded boxes indicate the mean and uncertainty for w across each redshift range. In both cases, information from BAO, SN Ia, and Hubble constant (BSH) measurements is combined with the *Planck* data. Also shown in the left panel is the result when information from measurements of weak lensing (WL) and redshift-space distortions (RSD) is used instead. Reproduced with permission from [92]. A and A © ESO, 2016.

$$\rho_{\rm de}(z) = \frac{3}{8\pi G}\left[\frac{1}{(\mathrm{d}r/\mathrm{d}z)^2} - \Omega_m H_0^2(1+z)^3\right]. \tag{25}$$

Direct reconstruction in its conceptual form is truly model-independent, in the sense that it does not require any assumptions about the functional form of time variation of dark energy density. However, to make it possible in practice, one has to regularize the distance derivatives, since these are derivatives of noisy data. One must fit the distance data with a smooth function (e.g. a polynomial, a Padé approximant, or a spline with tension), and the fitting process introduces systematic biases. While a variety of methods have been pursued [10, 98], the consensus is that direct reconstruction is simply not robust even with SN Ia data of excellent quality. Nevertheless, sufficiently strong priors on the behavior of the equation of state, coupled with advanced statistical treatments, can lead to successful (though somewhat smoothing-model dependent) reconstructions of $w(z)$ [99–103].

Although the expression for $\rho_{\rm de}(z)$ involves only first derivatives of $r(z)$ and is therefore easier to reconstruct, it contains little information about the nature of dark energy. Dark energy reconstruction methods have been reviewed in [12].

4.6. Figures of merit

It is useful to quantify the power of some probe, survey, or combination thereof, to measure dark energy properties. This is typically achieved by defining some function of the error bars or covariances of parameters describing dark energy and calling it the 'figure of merit' (FoM). Such a quantity necessarily only paints a limited picture of the power of some probe or experiment because it is a single number whose relative size depends on its very definition (for example, the weighting of dark energy properties in redshift). Nevertheless, FoMs, if judiciously chosen, are useful since they can dramatically simplify considerations about various survey specifications or survey complementarities.

The most commonly adopted figure of merit is that proposed by the Dark Energy Task Force ([104]; see [10] for the original proposal). This DETF FoM is the inverse of the allowed area in the w_0–w_a plane. For uncorrelated w_0 and w_a, this quantity would be $\propto 1/(\sigma_{w_0}\,\sigma_{w_a})$; because these two parameters are typically correlated, the FoM can be defined as

$$\mathrm{FoM} \equiv |\mathbf{C}|^{-1/2} \approx \frac{6.17\pi}{A_{95}}, \tag{26}$$

where $\mathbf{C}$ is the 2×2 covariance matrix for (w_0, w_a) after marginalizing over all other parameters, and A_{95} is the area of the 95.4% CL region in the w_0–w_a plane. Note that the constant of proportionality is not important; when we compare FoMs for different surveys, we consider the FoM ratio in which the constant disappears.

While the DETF FoM defined in (26) contains some information about the dynamics of dark energy (that is, the time variation of $w(z)$), several more general FoMs have been proposed. For example, a more general FoM is inversely proportional to the volume of the n-dimensional ellipsoid in the space of principal component parameters; $\mathrm{FoM}_n^{\mathrm{PC}} \equiv \left(|\mathbf{C}_n|/|\mathbf{C}_n^{\mathrm{prior}}|\right)^{-1/2}$ [105], where the prior covariance matrix is again unimportant since it cancels out when computing FoM ratios.

4.7. Generalized dark energy phenomenology

The simplest and by far the most studied class of models is dark energy that is spatially smooth and its only degree of freedom is its energy density—that is, it is fully described by either $\rho_{\mathrm{de}}(a)$ or $w(a) \sim -1$. More general possibilities exist however, as the stress-energy tensor allows considerably more freedom [106, 107].

One possibility is that dark energy has the speed of sound that allows clustering at sub-horizon scales, that is, $c_s^2 \equiv \delta p_{\mathrm{de}}/\delta\rho_{\mathrm{de}} < 1$ (where c_s is quoted in units of the speed of light) [108–111]. Unfortunately, the effects of the speed of sound are small, and become essentially negligible in the limit when the equation of state of dark energy w becomes close to -1, and are difficult to discern with late-universe measurements even if w deviates from the cosmological constant value at some epoch. It will therefore be essentially impossible to measure the speed of sound even with future surveys; see illustrations of the changes in the observables and forecasts in [112].

Another possibility is the presence of 'early dark energy' [113–115], component that is non-negligible at early times, typically around recombination or even earlier. The early component is motivated by various theoretical models (e.g. scalar fields [116]), and could imprint signatures via the early-time Integrated Sachs-Wolfe effect. While the *acceleration* in the redshift range $z \in [1, 10^5]$ is already ruled out [117], of order a percent contribution to the energy budget by early dark energy is still allowed [92, 118]. In some models, this early component this component acts like radiation in the early universe [119]. Increasingly good constraints on models with early dark energy are on the to-do list for upcoming cosmological probes.

Finally, there is a possibility that dark energy is coupled to dark matter, or other components or particles (some of the early work is in e.g. [120–122]). This is a much richer—though typically very model-dependent—set of possibilities, with many opportunities to test them using data; see [123] for a review.

As yet, there is no observational evidence for generalized dark energy beyond the simplest model but, as with modified gravity, studying these extensions is important to understand how dark energy phenomenology can be searched for by cosmological probes.

4.8. Descriptions of modified gravity

Modifications of general theory of relativity represent a fundamental alternative in describing the apparent acceleration to the smooth fluid description with a negative equation of state. In modified gravity (reviewed in this volume by Brax), the modification of GR makes an order-unity change in the dynamics at cosmological scales. At the solar-system scales, the modification of gravity needs to have a very small or negligible effect—usually satisfied by invoking non-linear 'screening mechanisms' which restore GR in high density regions—in order to respect the successful local tests of GR. There exists a diverse set of proposed modified gravity theories, with very rich set of potentially new cosmological signatures; for excellent reviews, see [124–126].

Modified gravity affects the clustering of galaxies and changes how mass affects the propagation of light. One can write the metric perturbations via two potentials Φ and Ψ as

$$\mathrm{d}s^2 = (1 + 2\Psi)\,\mathrm{d}t^2 - (1 - 2\Phi)\,a^2(t)\mathrm{d}\mathbf{x}^2. \tag{27}$$

A fairly general way to parametrize modified gravity theories is to specify the relation of the two metric potentials Φ and Ψ, which govern the motion of matter and of light, respectively. One possible parametrization is [127]

$$\nabla^2\Psi = 4\pi G_N a^2 \delta\rho\, G_{\mathrm{matter}} \tag{28}$$

$$\nabla^2(\Phi + \Psi) = 8\pi G_N a^2 \delta\rho\, G_{\mathrm{light}} \tag{29}$$

where deviations of dimensionless numbers G_{matter} or G_{light} from unity indicate at the very least clustering of dark energy, while $G_{\mathrm{matter}} \neq G_{\mathrm{light}}$ rather robustly alerts us to possible modifications of General Relativity. There is a surprisingly large number of equivalent parametrization conventions in the literature; they use different symbols, but all effectively describe the difference and ratio of the two gravitational potentials (e.g. [128–130]). The scale- and time-dependence of these parameters can be modeled with independent (z, k) bins [127], eigenmodes [131], or well behaved functional forms [132–135]. Note that the parametrization in equations (28) and (29) (and its various equivalents) is valid on subhorizon scales and in the linear regime, and does not capture the various screening mechanisms.

There exist various ways of testing gravity which stop short of modeling the two gravitational potentials, and are therefore potentially simpler to implement. The simplest such parametrization uses the growth index γ, defined in (12); any evidence for $\gamma \neq 0.55$ would point to departures from the standard cosmological ΛCDM model [136]. Other examples are statistics constructed to be closely related to the observables measured; for example, the E_G statistic [137, 138] is a suitably defined ratio of the galaxy–galaxy lensing clustering amplitude to that of galaxy clustering, and it allows a relatively direct link to the modified gravity parameters.

4.9. Consistency tests of the standard model

Finally, there are powerful but more phenomenological methods of testing the consistency of the current cosmological model that do not refer to explicit parametrizations of modified gravity theory. The general idea behind such tests is to begin with some widely adopted parametrization of the cosmological model (say, the ~5-parameter ΛCDM), then investigate whether there exist observations that are inconsistent with the theoretical predictions of the model. Bayesian statistical tools [139–145] are particularly useful to quantify these consistency tests.

The simplest approach is to calculate predictions on cosmological functions that can be measured that are consistent with current parameter constraints [86, 146, 147]. The predictions depend on the class of models that one is trying to test; for example, predictions for weak lensing shear power spectrum that assume an underlying ΛCDM model are tighter than the weak-lensing predictions that assume an evolving scalar field model where the equation of state of dark energy is a free function of time. Such model-dependent predictions for the observed quantities are now routinely employed in cosmological data analysis, as they provide a useful check of whether the newly obtained data fall within those predictions (e.g. [30]).

A complementary approach is to explicitly split the cosmological parameters into those constrained by geometry (e.g, distances, as in SNIa and BAO), and those constrained by the growth of structure (e.g. the evolution of clustering amplitude in redshift) [148–150]. In this approach, the equation of state of dark energy w, for example, can be split into two separate parameters, $w_{\rm geom}$ and $w_{\rm grow}$. These two parameters are then employed in those terms in theory equations that are based on geometry and growth, respectively. In this scheme, the principal hypothesis being tested is whether $w_{\rm geom} = w_{\rm grow}$. This so-called growth-geometry split allows explicit insights into what the data is telling us in case there is tension with ΛCDM, as this currently favored model makes very precise predictions about the relation between the growth and geometry quantities. For example, the currently discussed discrepancy between the measurement of the amplitude of mass fluctuations between the CMB and weak lensing (e.g. [151]) can be understood more clearly as the fact that the growth of structure—from current data, and not (yet) at an overwhelming statistical significance—is even more suppressed than predicted in the standard cosmological model, as the geometry-growth analysis indicates [152, 153]. Future cosmological constraints that incorporate an impressive range of probes with complementary physics sensitive to dark energy will be a particularly good test bed for the geometry-growth split analyses.

5. Principal probes of dark energy

In this section, we review the classic, principal cosmological probes of dark energy. What criterion makes a probe 'primary' is admittedly somewhat arbitrary; here we single out and describe the most mature probes of dark energy: type Ia supernovae (SNe Ia), the baryon acoustic oscillations (BAO), the cosmic microwave background (CMB), weak lensing, and galaxy clusters. We briefly review the history of these probes and discuss their current status and future potential. In the following section (section 6), we will discuss other probes of dark energy. Finally, in table 1 we summarize the primary and secondary probes of dark energy, along with their principal strengths and weaknesses.

5.1. Type Ia supernovae

Type Ia supernovae (SNe Ia) are very bright standard candles (sometimes called *standardizable* candles) useful for measuring cosmological distances. Below we discuss why standard candles are useful and then go on to review cosmology with SNe Ia, including a brief discussion of systematic errors and recent progress.

5.1.1. Standard candles. Distances in astronomy are often notoriously difficult to measure. It is relatively straightforward to measure the angular location of an object in the sky, and we can often obtain a precise measurement of an object's redshift z from its spectrum by observing the shift of known spectral lines due to the expansion of the universe ($1 + z \equiv \lambda_{\rm obs}/\lambda_{\rm emit}$). For a specified cosmological model, the distance-redshift relation (i.e. (8)) would then indicate the distance; however, since our goal is typically to *infer* the cosmological model, we need an *independent* distance measurement. Methods of independently measuring distance in astronomy typically involve uncertain empirical relationships. To measure the (absolute) distance to an object, such as a galaxy, astronomers have to construct a potentially unwieldy 'distance ladder'. For instance, they may employ relatively direct parallax measurements (apparent shifts due to Earth's motion around the Sun) to measure distances to nearby objects in our galaxy (e.g. Cepheid variable stars), then use those objects to measure distances to other nearby galaxies (for Cepheids, the empirical relation between pulsation period and intrinsic luminosity is the key). If systematic errors add up at each rung, the distance ladder will become flimsy.

Standard candles are idealized objects that have a fixed intrinsic luminosity or absolute magnitude [154]. Having standard candles would be very useful; they would allow us to infer distances to those objects using only the inverse square law for flux (recall that $f = L/(4\pi d_L^2)$, where d_L is the luminosity distance). In fact, we do not even need to know the luminosity of the standard candle when determining *relative* distances for a set of objects is sufficient. Observationally, flux is typically quantified logarithmically (the apparent magnitude), while luminosity is related to the absolute magnitude of the object. We therefore have the relation

$$m - M = 5\log_{10}\left(\frac{d_L}{10\ \mathrm{pc}}\right), \tag{30}$$

where the quantity $m - M$ is known as the distance modulus. For an object that is 10 pc away, the distance modulus is zero. For a true standard candle, the absolute magnitude M is the same for each object. Therefore, for each object, a measurement of the apparent magnitude provides direct information about the luminosity distance and therefore some information about the cosmological model.

5.1.2. Cosmology with SNe Ia. Supernovae are energetic stellar explosions, often visible from distant corners of the universe. Unlike other types of supernovae, which result from the core collapse of a massive, dying star, a type Ia supernova is thought to occur when a slowly rotating carbon-oxygen white dwarf accretes matter from a companion star, eventually exceeds the Chandrasekhar mass limit ($\sim 1.4 M_\odot$), and subsequently collapses and explodes[7]. The empirical SN classification scheme is based on spectral features, and type Ia SNe are characterized by a lack of hydrogen lines and the presence of a singly ionized silicon (Si II) line at 6150 Å. The flux of light from SNe Ia increases and then fades over a period of about a month; at its peak flux, a SN can be as luminous as the entire galaxy in which it resides.

SNe Ia had been studied extensively by Fritz Zwicky (e.g. [157]), who gave them their name and noted that SNe Ia have roughly uniform luminosities. The fact that SNe Ia can potentially be used as standard candles had been realized long ago, at least since the 1970s [158, 159]. However, developing an observing strategy to detect SNe Ia before they reached peak flux was a major challenge. If we were to point a telescope at a single galaxy and wait for a SN to occur, we would have to wait $\sim$100 years, on average. A program in the 1980s to find SNe [160] discovered only one, and even then, only after the peak of the light curve. Today, after many dedicated observational programs, thousands of SNe Ia have been observed, and nearly one thousand have been analyzed simultaneously for cosmological inference.

Of course, SNe Ia are not perfect standard candles; their peak magnitudes exhibit a scatter of $\sim$0.3 mag, limiting their usefulness as distance indicators. We now understand that much of this scatter can be explained by empirical correlations between the SN peak magnitude and both the *stretch* (broadness, decline time) of the light-curve and the SN color (e.g. the difference between magnitudes in two bands). Simply put, broader is brighter, and bluer is brighter. While the astrophysical mechanisms responsible for these relationships are somewhat uncertain, much of the color relation can be explained by dust extinction. After correcting the SN peak magnitudes for these relations, the intrinsic scatter decreases to $\lesssim$0.15 mag, allowing distance measurements with $\sim 7 - 10\%$ precision.

We can rewrite (30) and include the stretch and color corrections to the apparent magnitude:

$$5\log_{10}\left[\frac{H_0}{c}\, d_L(z_i, \mathbf{p})\right] = m_i + \alpha\, s_i - \beta\, C_i - \mathcal{M},$$

where m_i, s_i, and C_i are the observed peak magnitude, stretch, and color, respectively, for the ith SN. The exact definitions of these measures are specific to the light-curve fitting method employed (e.g. SALT2 [161]). Meanwhile, α, β, and $\mathcal{M}$ are 'nuisance' parameters that can be constrained simultaneously with the cosmological parameters $\mathbf{p}$. The $\mathcal{M}$ parameter,

$$\mathcal{M} \equiv M + 5\log_{10}\left[\frac{c}{H_0 \times 1\ \mathrm{Mpc}}\right] + 25,$$

is the Hubble diagram offset, representing a combination of *two* quantities which are unknown *a priori*, the SN Ia absolute magnitude M and the Hubble constant H_0. Their combination $\mathcal{M}$ can be constrained, often precisely, by SN Ia data alone, and one can marginalize over $\mathcal{M}$ to obtain constraints on the cosmological parameters $\mathbf{p}$. Note that H_0 and M *cannot* be individually constrained using SN data only, though external information about one of them allows a determination of the other.

Figure 3 is referred to as a Hubble diagram, and it illustrates the remarkable ability of SNe Ia to distinguish between various cosmological models that affect the expansion rate of the universe.

The original discovery of dark energy discussed in section 2 involved the crucial addition of a higher-redshift SN sample to a separate low-redshift sample. Results since then have improved gradually as more and more SNe have been observed and analyzed simultaneously (e.g. [162, 163]). Meanwhile, other cosmological probes (e.g. CMB, BAO; see figure 9) have matured and have independently confirmed the SN Ia results indicating the presence of a Λ-like dark energy fluid.

5.1.3. Systematic errors and recent progress. Recent SN Ia analyses (e.g. [164]) have focused on carefully accounting for a number of systematic uncertainties. These uncertainties can typically be included as additional (off-diagonal) contributions to the covariance matrix of SN distance moduli. As the number of observed SNe grows and statistical errors shrink, reducing the systematic uncertainties is key for continued progress and precision dark energy measurements.

Photometric calibration errors are typically the largest contribution to current systematic uncertainty budgets. In order to compare peak magnitudes of different SNe and interpret the difference as a relative distance, it is crucial to precisely understand any variation in the fraction of photons, originating from the SNe, that ultimately reach the detector. This category includes both photometric bandpass uncertainties and zero-point uncertainties. Part of the challenge is that current SN compilations consist of multiple subsamples, each

[7] While a white dwarf is always involved, other details of the progenitor system, or of the nuclear ignition and burning mechanism, are far from certain. It seems to be the case that many SNe Ia result from a merger between two white dwarfs (double degenerate progenitors), and there may be more diversity in the type of companion star than once thought (e.g. [155, 156]).

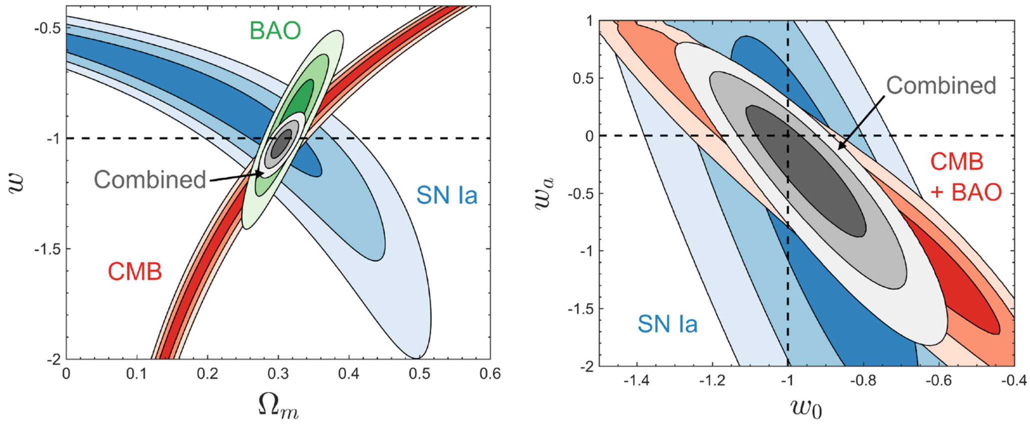

Figure 9. Constraints on cosmological parameters from our analysis of current data from three principal probes: SN Ia (JLA [203]; blue), BAO (BOSS DR12 [30]; green), and CMB (*Planck* 2015 [74]; red). We show constraints on Ω_m and constant w (left panel) and on w_0 and w_a in the parametrization from (17), marginalized over Ω_m (right panel). The contours contain 68.3%, 95.4%, and 99.7% of the likelihood, and we assume a flat universe in both cases.

observed with different instruments and calibrated using a different photometric system. This is a limitation which future large, homogeneous SN surveys will likely overcome, though it is also possible to reduce this uncertainty through consistent, precise recalibration of the existing samples [29].

Other contributions to the systematic error budget include uncertainties in the correction of bias resulting from selection effects (e.g. Malmquist bias), uncertainties in the correction for Milky Way dust extinction, uncertainty accounting for possible intrinsic evolution of SNe Ia or of the stretch and color relations, uncertainty due to contamination of the sample by non-Ia SNe (important for photometrically-classified SNe), uncertainty in K-corrections, gravitational lensing dispersion (primarily affecting high-redshift SNe [165]), peculiar velocities (important for low-redshift SNe), and uncertainty in host galaxy relations. Although there are numerous sources of systematic error, most are currently a sub-dominant contribution to the error budget, and the systematic effects themselves have by now been well studied. While systematic uncertainties are *not* trivially reduced by obtaining a larger SN sample, future surveys featuring better observations will likely reduce these errors further.

Other recent efforts have focused on improving the analysis of SN Ia data in preparation for the large samples expected in the future (e.g. LSST, WFIRST). This work has included the development of Bayesian methods for properly estimating cosmological parameters from SN Ia data [166, 167], including methods applicable to large photometrically-classified samples that will be contaminated by non-Ia SNe, which would otherwise bias cosmological measurements [168–170]. There are also techniques employing rigorous simulations to correct for selection and other biases and more accurately model SN Ia uncertainties [171, 172]. Meanwhile, new, detailed observations of individual SNe can help us identify subclasses of SNe Ia and determine the extent to which they may bias dark energy measurements [173–175]. Finally, it may be possible to reduce the effective intrinsic scatter by identifying specific SNe which are more alike than others [176] or by understanding how other observables, such as host galaxy properties, affect inferred SN luminosities.

For present SN Ia analyses, known systematic uncertainties have been quantified and are comparable to, or less than, the statistical errors. The fact that other, independent probes (BAO and CMB; see below) agree quantitatively with SN Ia results is certainly reassuring. Indeed, even if one completely ignores the SN data, the combination of the CMB distance with BAO data firmly points to a nearly flat universe with a subcritical matter density, thereby indicating the presence of a dark energy component.

5.2. Baryon acoustic oscillations

Baryon acoustic oscillations (BAO) refer to the wiggles in the matter power spectrum due to the coherent oscillations in the baryon-photon fluid in the epoch prior to recombination. The effect, first predicted nearly 50 years ago [177, 178], results in excess probability of a galaxy having a neighbor separated by the sound-horizon distance. This therefore implies a single acoustic peak in the configuration space clustering of galaxies at separation $r_s \simeq 100\ h^{-1}$Mpc or, equivalently, several ∼10% oscillations in the Fourier transform of the correlation function, that is, the matter power spectrum.

The power of BAO to probe dark energy comes from their exquisite power to measure the angular diameter distance to high redshift, as well as the Hubble parameter $H(z)$, using the sound horizon as a 'standard ruler'. The sound horizon is the radiation-era distance covered by the speed of sound, which is $c/\sqrt{3}$ with a correction for the non-negligible presence of baryons:

$$\begin{aligned} r_s &= \int_0^{t_*} \frac{c_s}{a(t)}\,\mathrm{d}t = \frac{c}{\sqrt{3}} \int_0^{a_*} \frac{\mathrm{d}a}{a^2 H(a)\sqrt{1+\frac{3\Omega_b}{4\Omega_\gamma}\,a}} \\ &= (144.6 \pm 0.5)\ \mathrm{Mpc}\,, \end{aligned} \tag{31}$$

where $a_* \sim 10^{-3}$ is the scale factor at recombination. The error quoted in (31) comes from *Planck* [74]; it is known independently to such a high precision due to measurements of the physical matter and baryon densities from the morphology of the peaks in the CMB angular power spectrum.

A pioneering detection of the BAO feature was made from analysis of the Sloan Digital Sky Survey (SDSS) galaxy data [179]. Much improvement has been made in subsequent measurements [180–187].

Measurement of the angular extent of the BAO feature, together with precise, independent knowledge of the sound horizon, enables determination of both the angular diameter distance to the redshift of the sample of galaxies and the Hubble parameter evaluated at that epoch [188–190]. More specifically, clustering of the galaxies in the transverse direction can be used to measure the angular diameter distance to the characteristic redshift of the galaxy sample,

$$\Delta\theta_s = \frac{r_s}{d_{\rm A}(z)} \quad \text{(transverse modes)}. \tag{32}$$

Meanwhile, clustering in the radial direction constrains the Hubble parameter at the same redshift since the redshift extent of the BAO feature Δz_s is effectively observed; it is related to the Hubble parameter via

$$\Delta z_s = \frac{H(z)\, r_s}{c} \quad \text{(radial modes)}. \tag{33}$$

Radial modes are particularly helpful, as they provide localized information about dark energy via the Hubble parameter at redshift of the galaxy sample. However, radial modes are also more difficult to measure than the transverse modes, essentially because the transverse modes span a two-dimensional space while radial modes live in only one dimension. Up until recently, the BAO measurements had sufficiently large statistical error that it was a good approximation to constrain the generalized distance that combines the transverse and radial information [179]

$$D_V(z) \equiv \left[(1+z)^2 d_{\rm A}(z) \frac{cz}{H(z)}\right]^{1/3}. \tag{34}$$

With current or future data, separating into transverse and radial modes is feasible, and enables extracting more information about dark energy.

The main strength of the BAO comes from its excellent theoretical foundation: the physics of the acoustic oscillations is exceptionally well understood. While the systematic errors do affect the amplitudes and, to a lesser extent, positions of the acoustic peaks in the galaxy power spectrum, these shifts are largely correctable. In particular, nonlinear clustering, strongly subdominant at scales $\simeq$100 h^{-1}Mpc, shifts the peak positions by only a fraction of one percent [191, 192], and even that small shift can be accurately predicted—and therefore modeled—using a combination of theory and simulations [193]. Nevertheless, a mild concern remains the possibility that galaxy density is modulated by non-gravitational effects on scales of $\simeq$100 h^{-1}Mpc, which in principle shifts the peaks by small but non-negligible amount. Such large-scale modulation could be caused, for example, by the fact that galaxies are biased tracers of the large-scale structure (for a review, see [194]).

The most powerful BAO experiments necessarily need to be spectroscopic surveys, as the required redshift accuracy in order not to smear the BAO feature corresponds to a few percent of the BAO standard ruler r_s, meaning a few megaparsecs or $\delta z \lesssim 0.001$. (Low-resolution BAO measurements are possible with photometric surveys with sufficiently accurate photometric redshifts.) Another requirement is large volume, so that sufficiently many samples of the sound-horizon feature can be mapped, and sample variance suppressed. Prime Focus Spectrograph (PFS; [195]) and Dark Energy Spectroscopic Instrument (DESI; [196, 197]) represent important future surveys whose principal goal is to maximize the BAO science and obtain excellent constraints on dark energy.

Tracers other than galaxies or quasars can be used to detect and utilize the BAO feature. For example, Lyman alpha forest is useful in mapping structure in the universe; these are the ubiquitous absorption lines seen in high-resolution spectra of distant quasars or galaxies due to hydrogen gas clouds and filaments along the line of sight which show up as 'trees' in the forest. Lyman-alpha systems are challenging to model since a variety of physical processes, including hydrogen recombination, radiative heating, and photo-ionization need to be known, often using simulations. However the BAO feature, being at ~100Mpc scale, is considered more robust, and has actually been detected in the Lyman-alpha forest and used to constrain the angular diameter distance and Hubble parameter at $z \sim 2$, deep in the matter-dominated era [198–202].

Finally, note that the BAO measurements provide an *absolute* distance measurement, in the limit when the sound horizon r_s is perfectly known from e.g. the morphology of the CMB peaks (recall that SNIa provide relative distances since the vertical offset in the SN Hubble diagram, or equivalently the Hubble constant, is marginalized over). This makes BAO not only complementary to SNIa, but also powerful in connecting the low-z and high-z measurements of the expansion history. Current BAO constraints on key dark energy parameters are shown in figure 9.

5.3. Cosmic microwave background radiation

While otherwise known as a Rosetta Stone of cosmology for its ability to constrain cosmological parameters to spectacular precision [204, 205], the cosmic microwave background at first appears disappointingly insensitive to dark energy. This naïve expectation is borne out because the physics of the CMB takes place in the early universe, well before dark energy becomes important. There, baryons and photons are coupled due to the Coulomb coupling between protons and electrons and the Thomson scattering between electrons and photons. This coupling leads to coherent oscillations, which in turn manifest themselves as wiggles in the observed power in the distribution of the hot and cold spots on the microwave sky. The angular power spectrum that describes the statistical distribution of the temperature anisotropies (see the lower left panel in figure 5) therefore has rich structure that can be fully predicted as a function of cosmological parameters to sub-percent-level accuracy. The angular power spectrum is a superb source of information about, not only the inflationary parameters, but also dark matter and even, as we discuss here, dark energy.

Dark energy affects the distance to the epoch of recombination, and therefore the angular scale at which the CMB fluctuations are observed. This sensitivity is precisely the reason why the CMB is in fact a very important complementary probe of dark energy. Given that the physics of the CMB takes place at the redshift of recombination when dark energy is presumably completely negligible, the physical structure of CMB fluctuations is unaffected by dark energy, as long as we do not consider the early dark energy models with significant early contribution to the cosmic energy budget. The sound horizon r_s, defined in (31), is projected to angle

$$\theta_* = \frac{r_s(z_*)}{r(z_*)}, \tag{35}$$

where z_* is the recombination redshift and r is the comoving distance (8). The latter quantity is affected by dark energy at $z \lesssim 1$ (see figure 5). Therefore, dark energy affects the angle at which the features are observed—that is, the horizontal location of the CMB angular power spectrum peaks. More dark energy (higher $\Omega_{\rm de}$) increases $d_{\rm A}$ and therefore shifts the CMB pattern to smaller scales, and vice versa.

To the extent that the CMB provides a single but *very* precise measurement of the peak location, it provides a very important complementary constraint on the dark energy parameters. In a flat universe, the CMB thus constrains a degenerate combination of Ω_m and w (and, optionally, w_a or other parameters describing the dark energy sector). While the CMB appears to constrain just another distance measurement—much like SNe Ia or BAO, albeit at a very high redshift ($z_* \simeq 1000$)—its key advantage is that the $d_{\rm A}$ measurement comes with $\Omega_m h^2$ essentially fixed by features in the CMB power spectrum. In other words, the CMB essentially constrains the comoving distance to recombination with the physical matter density $\Omega_m H_0^2$ fixed [206],

$$R \equiv \sqrt{\Omega_m H_0^2}\; r(z_*), \tag{36}$$

which is sometimes referred to as the 'CMB shift parameter' [96, 207]. Because of the fact that $\Omega_m h^2$ is effectively factored out, the CMB probes a different combination of dark energy parameters than SNe or BAO at any redshift. In particular, the combination of Ω_m and w constrained by the CMB is approximately [208] $D \equiv \Omega_m - 0.94\,\overline{\Omega}_m\,(w - \overline{w})$ where $(\overline{\Omega}_m, \overline{w}) \simeq (0.3, -1)$. This combination is measured with few-percent-level precision by *Planck*; see figure 9. It drastically reduces the parameter errors when combined with other probes [208] despite the fact that the CMB peak positions cannot constrain the dark energy parameters on their own (the lensing pattern in the CMB, however, is independently sensitive to dark energy [209]). Important complementary constraints on dark energy have been provided by several generations of CMB experiments, including tBoomerang, Maxima and DASI [210, 211], *WMAP* [212–216], *Planck* [74, 217], and also CMB experiments that probe smaller angular scales such as ACT and SPT [218, 219].

Another, much weaker, effect of dark energy on the CMB power spectrum is through the late-time Integrated Sachs Wolfe (ISW) effect [220, 221]. The ISW is due to the change in the depth of the potential wells when the universe is not matter dominated. One such epoch—the *early-time* ISW effect—occurs around recombination when radiation is not yet completely negligible. The *late-time* ISW effect occurs when dark energy becomes important at $z \lesssim 1$. The late-time ISW produces additional power in the CMB power spectrum at very large angular scales—multipoles $\lesssim$20, corresponding to scales larger than about 10 degrees on the sky. There is an additional dependence on the speed of sound of the dark energy fluid; however this effect becomes negligible as $w \to -1$, leaving only the overall effect of smooth dark energy [110, 222, 223]. Unfortunately the cosmic variance error is large at these scales, leading to very limited extent to which the late-time ISW can be measured. Nevertheless, it is important to account for the ISW when producing theory predictions of various dark energy models; for example, modified gravity explanations for the accelerating universe often predict specific ISW signatures [224].

5.4. Weak gravitational lensing

Gravitational lensing—bending of light by mass along the line of sight to the observed source—is theoretically well understood and also readily observed, and therefore represents a powerful probe of both geometry and structure in the universe. The principal advantage of lensing (relative to e.g. observations of galaxy clustering) is that lensing is fundamentally independent of the prescription of how the observed halos or galaxies trace the underlying dark matter—the so-called 'bias'. While most of the manifestations of gravitational lensing are sensitive to dark energy, we here describe weak lensing as the principal probe. In section 6 we also discuss the so-called strong lensing, galaxy–galaxy lensing, and counting of the peaks in the shear field as additional, complementary lensing probes of the accelerating universe.

Weak gravitational lensing is bending of light by structures in the Universe; it leads to distorted or sheared images of distant galaxies, see the left panel of figure 10. This distortion allows the distribution of dark matter and its evolution with time to be measured, thereby probing the influence of dark energy on the growth of structure (for a detailed review, see e.g. [225]; for brief reviews, see [226] and [227]).

Gravitational lensing produces distortions of images of background galaxies. These distortions can be described as mapping between the source plane (S) and image plane (I),

$$\delta x_i^S = A_{ij}\delta x_j^I, \tag{37}$$

where $\delta\mathbf{x}$ are the displacement vectors in the two planes and A is the distortion matrix,

$$A = \begin{pmatrix} 1-\kappa-\gamma_1 & -\gamma_2 \\ -\gamma_2 & 1-\kappa+\gamma_1 \end{pmatrix}. \tag{38}$$

The deformation is described by the convergence κ and complex shear (γ_1, γ_2); the total shear is defined as $|\gamma| = \sqrt{\gamma_1^2+\gamma_2^2}$. We are interested in the limit of weak lensing, where $\kappa, |\gamma| \ll 1$. The magnification of the source, also given in terms of κ and $\gamma_{1,2}$, is

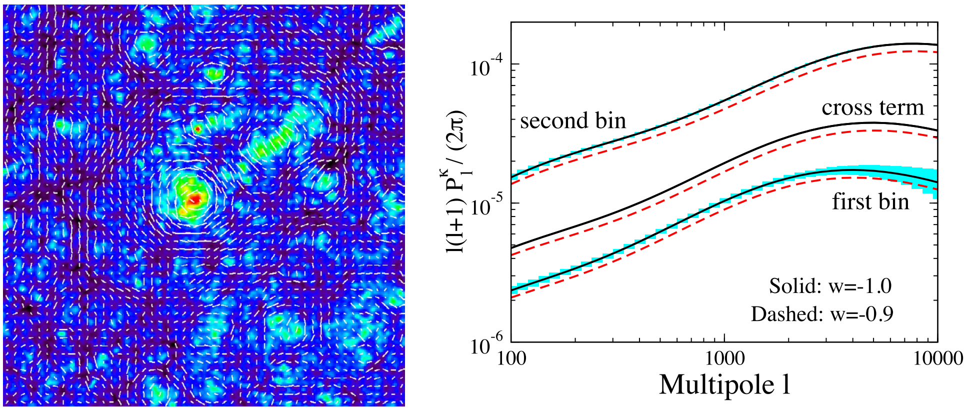

Figure 10. *Left panel*: Cosmic shear field (white whiskers) superimposed on the projected mass distribution from a cosmological *N*-body simulation, where overdense regions are bright and underdense regions are dark. Note how the shear field is correlated with the foreground mass distribution; the shears are azimuthal around overdensities and radial around underdensities. Figure courtesy of T. Hamana. *Right panel*: Angular power spectrum of cosmic shear along with statistical errors expected for LSST for two values of the dark energy equation-of-state parameter. For illustration, results are shown for source galaxies in two broad redshift bins, $0 < z_s < 1$ (first bin) and $1 < z_s < 3$ (second bin); the cross-power spectrum between the two bins (cross term) is shown without the statistical errors.

$$\mu = \frac{1}{|1-\kappa|^2 - |\gamma|^2} \approx 1 + 2\kappa + O(\kappa^2, \gamma^2), \qquad (39)$$

where the second, approximate relation holds in the weak lensing limit.

Given a sample of sources with known redshift distribution and cosmological parameter values, the convergence and shear can be predicted from theory. The convergence κ in any particular direction on the sky $\hat{\boldsymbol{n}}$ is given by the integral along the line of sight $\kappa(\hat{\boldsymbol{n}}, \chi) = \int_0^{\chi} W(\chi')\,\delta(\chi')\,\mathrm{d}\chi'$, where δ is the relative perturbation in matter energy density and $W(\chi)$ is the geometric weight function describing the lensing efficiency of foreground galaxies. The most efficient lenses lie about halfway between us and the source galaxies whose shapes we measure.

The statistical signal due to gravitational lensing by large-scale structure is termed ‘cosmic shear’. To estimate the cosmic shear field at a given point in the sky, we locally average the shapes of large numbers of distant galaxies. The principal statistical measure of cosmic shear is the shear angular power spectrum, which chiefly depends on the source galaxy redshift z_s, and additional information can be obtained by measuring the correlations between shears at different redshifts or with foreground lensing galaxies, as well as the *three*-point correlation function of cosmic shear [228].

The convergence can be transformed into multipole space $\kappa_{lm} = \int \mathrm{d}\hat{\boldsymbol{n}}\,\kappa(\hat{\boldsymbol{n}}, \chi)\,Y_{lm}^{*}(\hat{\boldsymbol{n}})$, and the power spectrum is defined as the two-point correlation function (of convergence, in this case) $\langle \kappa_{\ell m} \kappa_{\ell' m'} \rangle = \delta_{\ell\ell'}\,\delta_{mm'}\,P_\ell^\kappa$. The convergence[8] angular power spectrum is

$$P_\ell^\kappa(z_s) = \int_0^{z_s} \frac{\mathrm{d}z}{H(z) d_\mathrm{A}^2(z)} W(z)^2 P\left(k = \frac{\ell}{d_\mathrm{A}(z)}; z\right), \qquad (40)$$

where ℓ denotes the angular multipole, $d_\mathrm{A}(z) = (1+z)^{-2} d_L(z)$ is the angular diameter distance, the weight function $W(z)$ is the efficiency for lensing a population of source galaxies and is determined by the distance distributions of the source and lens galaxies, and $P(k, z)$ is the usual matter power spectrum. One important feature of (40) is the integral along the line of sight, which encodes the fact that weak lensing radially projects the density fluctuations between us and the sheared source galaxy. Additional information is obtained by measuring the shear correlations between objects in different redshift bins; this is referred to as weak lensing tomography [229] and contains further useful information about the evolution of the growth of structure.

The dark energy sensitivity of the shear angular power spectrum comes from two factors:

- *geometry*—the Hubble parameter, the angular diameter distance, and the weight function $W(z)$; and
- *growth of structure*—via the redshift evolution of the matter power spectrum $P(k)$ (more specifically, via the growth factor $D(z)$ in (10)).

Due to this two-fold sensitivity to dark energy and, in recent years, the advent of better-quality observations and larger surveys, weak lensing now places increasingly competitive constraints on dark energy [230–238].

The statistical uncertainty in measuring the shear power spectrum on large scales is

$$\Delta P_\ell^\kappa = \sqrt{\frac{2}{(2\ell+1) f_\mathrm{sky}}} \left[P_\ell^\kappa + \frac{\sigma^2(\gamma_i)}{n_\mathrm{eff}} \right], \qquad (41)$$

where f_sky is the fraction of sky area covered by the survey, σ_{γ_i} is the standard deviation in a single component of the (two-component) shear ($\sim$0.2 for typical measurements), and n_eff is the effective number density per steradian of galaxies with well-measured shapes. The first term in the brackets represents sample variance (also called *cosmic variance*), which arises due to the fact that only a finite number of independent samples of cosmic structures are available in our survey. This term dominates on larger scales. The second term, which dominates on small scales, represents shot noise from both the

[8] At lowest order, the convergence power spectrum is equal to the shear power spectrum.

variance in galaxy ellipticities ('shape noise') and the finite number of galaxies (hence the inverse proportionality to $n_{\rm eff}$).

Systematic errors in weak lensing measurements principally come from the limitations in accurately measuring galaxy shapes. These shear measurements are complicated by a variety of thorny effects such as the atmospheric blurring of the images, telescope distortions, charge transfer in CCDs, to name just a few. More generally, a given measurement of the galaxy shear will be subject to additive and multiplicative errors that affect the true shear [239, 240]. The weak lensing community has embarked on a series of challenges to develop algorithms and techniques to ameliorate these observational systematics (e.g. [241]). There are also systematic uncertainties due to limited knowledge of the redshifts of source galaxies: because taking spectroscopic redshifts of most source galaxies will be impossible (for upcoming surveys, that number will be of order a billion), the community has developed approximate photometric redshift techniques, where one obtains a noisy redshift estimate from multi-wavelength (i.e. multi-color) observations of each galaxy. In order for the photometric redshift biases not to degrade future dark energy constraints, their mean calibration at the 0.1% level will be required [242, 243].

The interpretation of weak lensing measurements also faces theoretical challenges, such as the need to have accurate predictions for clustering in the non-linear regime from N-body simulations [244–246] and to account for non-Gaussian errors on small angular scales [247–249]. Finally, intrinsic alignments of galaxy shapes, due to tidal gravitational fields, are a serious contaminant which requires careful modeling as well as external astrophysics input, such as observationally-inferred galaxy separation, type, and luminosity information; for a review, see [250].

The right panel of figure 10 shows the weak lensing shear power spectrum for two values of w, and the corresponding statistical errors expected for a survey such as LSST, assuming a survey area of 15 000 deg^2 and effective source galaxy density of $n_{\rm eff} = 30$ galaxies per square arcminute, and divided into two radial slices. Current surveys cover more modest hundreds of deg^2, although KIDS (450, and soon to be up to 1500 deg^2 [237]), Dark Energy Survey (about 1500 and soon to be 5000 deg^2 [251]) and Hyper Suprime-Cam (HSC; expected to be 1500 deg^2 [252]) are aiming to bring weak lensing to the forefront of dark energy constraints. Note that the proportionality of errors to $f_{\rm sky}^{-1/2}$ means that, as long as the systematic errors can be controlled, large sky coverage is at a premium. Further improvement in dark energy constraints can be achieved by judiciously combining a photometric and a spectroscopic survey [253–258].

The weak lensing signal can also be used to *detect* and count massive halos, particularly galaxy clusters. This method, pioneered recently [259, 260], can be used to obtain cluster samples whose masses are reliably determined, avoiding the arguably more difficult signal-to-mass conversions required with the x-ray or optical observations [261–264]. Much important information about the dark matter and gas content of galaxy clusters can be inferred with the combined lensing, x-ray, and optical observations. This has recently been demonstrated with observations of the 'Bullet Cluster' [265], where the dark matter distribution inferred from weak lensing is clearly offset from the hot gas inferred from the x-ray observations, indicating the presence and distinctive fingerprints of dark matter.

5.5. Galaxy clusters

Galaxy clusters—the largest collapsed objects in the universe with mass $\gtrsim 10^{14} M_\odot$ and size a few Mpc—are just simple enough that their spatial abundance and internal structure can be used to probe dark energy. Clusters are versatile probes of cosmology and astrophysics and have had an important role in the development of modern cosmology (for a review, see [266]). In the context of dark energy, one can use the spatial abundance of clusters and compare it to the theoretical expectation that includes the effects of dark energy. This classic test is in principle very simple, since the number density of clusters can be inferred from purely theoretical considerations or, more robustly, from suites of numerical simulations. In practice, however, there are important challenges to overcome.

The number of halos in the mass range $[M, M + {\rm d}M]$ in a patch of the sky with solid angle ${\rm d}\Omega$ and in redshift interval $[z, z + {\rm d}z]$ is given by

$$\frac{{\rm d}^2N}{{\rm d}\Omega {\rm d}z} = \frac{r^2(z)}{H(z)}\,\frac{{\rm d}n(M,z)}{{\rm d}M}\,{\rm d}M\,, \qquad (42)$$

where $r^2/H = {\rm d}V/({\rm d}\Omega {\rm d}z)$ is the comoving volume element and $n(M, z)$ is the number density (the 'mass function') that is calibrated with numerical simulations (e.g. [267]).

Assuming Gaussian initial conditions, the comoving number density of objects in an interval ${\rm d}M$ around mass M is

$$\frac{{\rm d}n}{{\rm d}\ln M} = \frac{\rho_{M,0}}{M}\left|\frac{{\rm d}F(M)}{{\rm d}\ln M}\right|\,, \qquad (43)$$

where $\rho_{M,0}$ is evaluated at the present time and $F(M)$ is the fraction of collapsed objects. The original analysis of Press and Schechter [268] assumed a Gaussian initial distribution of overdensities, leading to $F(M) = (1/2)\,{\rm erfc}(\nu/\sqrt{2})$, where $\nu(M) \equiv \delta_c/\sigma(M)$ is the peak height and $\delta_c = 1.686$ is the critical threshold for collapse in the spherical top-hat model [269]. The Press-Schechter formula also involves multiplying the mass function by the notorious overall factor of two to account for underdensities as well as overdensities. Subsequent work has put the theoretical estimates on considerably firmer footing (for a review, see [270]), but the most accurate results are based on fits to numerical simulations, which calibrate the mass function for the standard ΛCDM class of models to a precision of about 5% [271]. Smooth dark energy models described by the modified linear growth history via the equation of state $w(a)$ are still reasonably well fit with the standard ΛCDM formulae [272], while modified gravity models sometimes predict scale-dependent growth $D(a, k)$ even in the linear regime and must be calibrated by simulations specifically constructed for the given class of modified gravity models (for a review, see [273]).

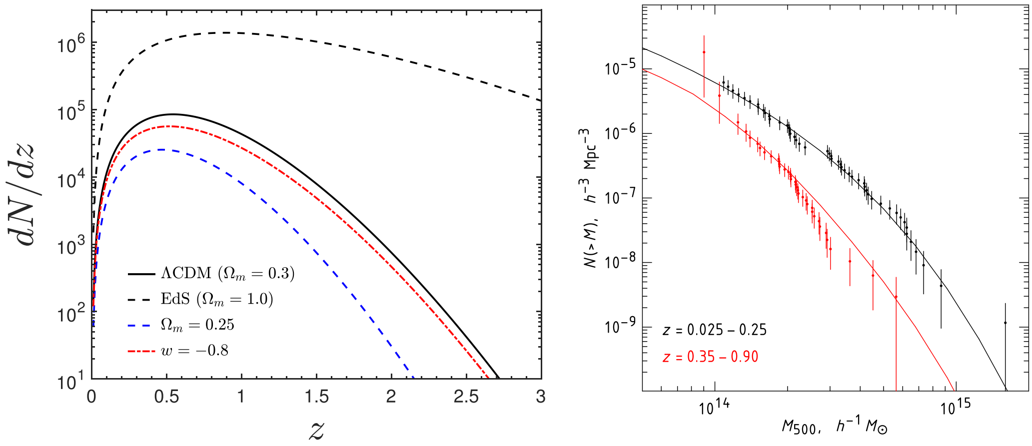

Figure 11. *Left panel*: Predicted cluster counts for a survey covering 5000 deg^2 that is sensitive to halos more massive than $10^{14}\ h^{-1}M_\odot$, shown for a fiducial ΛCDM model as well as three variations as in figure 5. *Right panel*: Measured mass function—$n(z, M_{\rm min}(z))$, in our notation—from the 400 deg^2 survey of ROSAT clusters followed up with the *Chandra* space telescope; reproduced from [274]. © IOP Publishing Ltd. All rights reserved.

The absolute number of clusters in a survey of solid angle $\Omega_{\rm survey}$ centered at redshift z and in the shell of thickness Δz is given by

$$N(z, \Delta z) = \Omega_{\rm survey} \int_{z-\Delta z/2}^{z+\Delta z/2} n(z, M_{\rm min}(z)) \frac{{\rm d}V(z)}{{\rm d}\Omega\,{\rm d}z}\,{\rm d}z\,, \qquad (44)$$

where $M_{\rm min}$ is the minimal mass of clusters in the survey. Note that knowledge of the minimal mass is extremely important, since the mass function $n(z, M_{\rm min}(z))$ decreases exponentially with M such that most of the contribution comes from a small range of masses just above $M_{\rm min}$. Recent cluster observations typically do not have enough signal-to-noise to determine the cluster masses directly; instead, forward-modeling can be applied to the mass function to recast the theory in the space of observable quantities [275]. One commonly used proxy for the cluster mass is the optical 'richness'—the number of galaxies per cluster—which is straightforward to measure from observations [276, 277].

The sensitivity of cluster counts to dark energy arises from the same two factors as in the case of weak lensing:

- *geometry*—the term ${\rm d}V(z)/({\rm d}\Omega\,{\rm d}z)$ in (44), which is the comoving volume element; and
- *growth of structure*—$n(z, M_{\rm min}(z))$ depends on the evolution of density perturbations.

The mass function's near-exponential dependence on the power spectrum in the high-mass limit is at the root of the power of clusters to probe the growth of density fluctuations. Specifically, the mass function is very sensitive to the amplitude of mass fluctuations smoothed on some scale R *calculated assuming linear theory*. That is,

$$\sigma^2(R, z) = \int_0^\infty \Delta^2(k, z) \left(\frac{3j_1(kR)}{kR}\right)^2 {\rm d}\ln k\,, \qquad (45)$$

where Δ^2 is the linear version of the power spectrum from (14) and R is traditionally taken to be 8 h^{-1} Mpc at $z = 0$, roughly corresponding to the characteristic size of galaxy clusters. The term in parentheses in the integrand is the Fourier transform of the top-hat window which averages out the perturbations over regions of radius R. The left panel of figure 11 shows the sensitivity of the cluster counts to the dark energy equation-of-state parameter, while the right panel shows measurements of the mass function based on x-ray observations [274].

There are other ways in which clusters can be used to probe dark energy. For example, their two-point correlation function probes the matter power spectrum as well as the growth and geometry factors sensitive to dark energy. Clusters can also be correlated with background galaxies to probe the growth ([278]; this is essentially a version of galaxy–galaxy lensing discussed in section 6). While these two tests can also be carried out using the much more numerous galaxies, clusters have the advantage of having more accurate individual photometric redshifts.

Clusters can be detected using light in the x-ray, optical, or millimeter waveband, or else using weak gravitational lensing of background galaxies behind the cluster. Some of these methods suffer from contamination due to the projected mass, as large-scale structures between us and the cluster contribute to the signal and can, in extreme cases, conspire to create appearance of a cluster from radially aligned, but dispersed, collections of numerous low-mass halos. This particularly affects detection of clusters via lensing (e.g. [279]). It is therefore necessary to use N-body simulations to calibrate purity (contribution of false detections) and completeness (fraction of detections relative to the truth) in these lensing observations [280, 281]. However, the possibility of cluster finding and mass inference in multiple wavebands is also a great strength of this probe, as it allows cross-checks and cross-calibrations, in particular of the cluster masses. Over the past decade, the wealth of ways to detect and characterize clusters, combined with improving ways to characterize the relation between their observable properties and mass, has led to increasingly interesting constraints on dark energy parameters [266, 274, 282–286]. Comparisons between dynamical and lensing cluster mass estimates are also sensitive to modifications of gravity [287].

Regardless of how the clusters are detected, the principal systematic concern is how to relate the observable quantity

Table 1. Comparison of dark energy probes. The five primary probes are the most mature, but a variety of other probes offer complementary information and have potential to provide important constraints on dark energy.

Probe/Method	Strengths	Weaknesses
	Primary probes of dark energy	
SN Ia	Pure geometry, model-independent, mature	Calibration, evolution, dust extinction
BAO	Pure geometry, low systematics	Requires millions of spectra
CMB	Breaks degeneracy, precise, low systematics	Single distance only
Weak lensing	Growth & geometry, no bias	measuring shapes, baryons, photo-z
Cluster counts	Growth & geometry, X-ray, SZ, & optical	mass-observable, selection function
	Other probes of dark energy	
Gal-gal lensing	High S/N	Bias, baryons
Strong lensing	Unique combination of distances	Lens modeling, structure along los
RSD	Lots of modes, probes growth	Theoretical modeling
Peculiar velocities	Probes growth, modified gravity	Selection effects, need distances
Hubble constant	Breaks degeneracy, model-independent	distance ladder systematics
Cosmic voids	Nearly linear, easy to find	galaxy tracer fidelity, consistent definition and selection
Shear peaks	Probes beyond 2-pt	Theoretical modeling versus projection
Galaxy ages	Sensitive to $H(z)$	Galaxy evolution, larger systematics
Standard sirens	High z, absolute distance	Optical counterpart needed for redshift, lensing
Redshift drift	Clean interpretation	Tiny signal, huge telescope, stability
GRB & quasars	Very high z	Standardizable?

(x-ray flux, Sunyaev–Zeldovich signal, lensing signature) to the mass of the cluster. In the past, the principal mass proxies have used x-ray observations and assumed hydrostatic equilibrium. Recurring concerns about the latter assumption imply significant statistical and systematic errors, and only tens of percent mass accuracy per cluster are achieved with these traditional approaches. Arguably the most secure method for determining the mass is weak gravitational lensing of source galaxies behind the cluster which, when possible, is combined with their strong lensing signatures. Such lensing efforts already enable a better than 10% mass accuracy per cluster [288–290]. The requirement on the individual mass precision, in order to be sufficient for future surveys, is approximately 2–5% [11].

A secondary source of systematics is the photometric redshifts of galaxy cluster members, which are combined to determine the redshift of the cluster. Averaging of individual redshifts fortunately leads to fairly accurate photometric redshift estimates, $\sigma_z/(1+z) \simeq 0.01$ (e.g. [291]), such that only moderate improvement is required for future dark energy constraints [292, 293].

Like other probes, clusters are amenable to determining the parameters describing the systematic errors internally from the data, the process known as self-calibration [294–296]. While any nuisance parameters can be self-calibrated, the most important uncertainty is typically tied to parameters that describe the scaling relations between mass and observable properties of the cluster (e.g. flux, temperature). Key to progress on the control of cluster systematics, as well as the program of self-calibration, is a multi-wavelength view of the clusters. Analyses that use a combination of weak and strong lensing signatures, as well as detections and observations in the optical, x-ray, and microwave (via the SZ effect), open many avenues for the robust use of clusters to probe geometry and growth evolution (e.g. [297]).

6. Other probes of dark energy

There are a number of powerful secondary probes of dark energy. While they do not quite have the power to individually impose strong constraints on dark energy without major concerns about the systematic errors, they provide complementary information, often hold a lot of promise, and sometimes come ‘for free’ with astrophysical or cosmological observations in surveys. Here we review some of the most promising of these methods.

6.1. Galaxy-galaxy lensing

Another effective application of weak lensing is to measure the correlation of the shear of background galaxies with the mass of the foreground galaxies. This method, which is referred to as ‘galaxy–galaxy lensing’ [298–307], essentially probes the galaxy-shear correlation function across the sky. Galaxy-galaxy lensing measures the surface mass density contrast $\Delta\Sigma(R)$,

$$\Delta\Sigma(R) \equiv \overline{\Sigma}(<R) - \overline{\Sigma}(R) = \Sigma_{\rm crit} \times \gamma_t(R)\,, \tag{46}$$

where $\overline{\Sigma}(<R)$ is the mean surface density within proper radius R, $\overline{\Sigma}(R)$ is the azimuthally averaged surface density at radius R (e.g. [308, 309]), γ_t is the tangentially-projected shear, and $\Sigma_{\rm crit}$ is the critical surface density, a known function of the distances to the source and the lens.

Current measurements constrain the density profiles and bias of dark matter halos [301, 310–312] as well as the relation between their masses and luminosities [313, 314]. In the future, galaxy-shear correlations have the potential to constrain dark energy models [315] and modified gravity models for the accelerating universe [316].

6.2. Strong gravitational lensing

Distant galaxies and quasars occasionally get multiply imaged due to intervening structure along the line of sight. While relatively rare—about one in a thousand objects is multiply imaged—strong lensing has the nice feature that, like weak lensing, it is sensitive to *all* matter in the universe and not just the visible part. There is a long history of trying to use counts of strongly lensed system to constrain the cosmological parameters [317–319]; however, its strong dependence on the independent knowledge of the density profile of lenses makes robustness of this approach extremely challenging to achieve. Instead, strong lensing time delays between images of the same source object offer a more promising way to constrain the Hubble constant [320] but also dark energy (e.g. [321, 322]). Time delays are sensitive to a unique combination of distances, sometimes called the time-delay distance [323]

$$D_{\Delta t} \equiv (1+z_l)\,\frac{d_{\rm A}(z_l)\,d_{\rm A}(z_s)}{d_{\rm A}(z_l,z_s)} = \frac{\Delta t}{\Delta\phi},$$

where z_l and z_s are the lens and source redshift respectively, Δt is the time delay, and $\Delta\phi$ is the so-called Fermat potential difference evaluated between different image locations. Because the Fermat potential can be constrained by lens modeling, the time-delay measurements measure $D_{\Delta t}$, which in turn offers dark energy parameter sensitivity that is complementary to that of other cosmological probes [324]. Additional information can be obtained by measurements of the velocity dispersion of lens galaxies, which effectively determine its mass; this, plus measurements of the gravitational potential, determine the size of the lens, which can then be used as a standard ruler and provide information about $d_{\rm A}(z_l)$ [325, 326] and thus dark energy [327]. Strong lensing time delays are reviewed in [328].

6.3. Redshift-space distortions (RSD)

On large scales, peculiar velocities of galaxies are affected by gravitational potential of the large-scale structures in a coherent, quantifiable way. In linear theory, the gradient of the velocity is proportional to the overdensity, $\nabla\cdot\mathbf{v}(\mathbf{r}) = -(aH)f\delta(\mathbf{r})$, where $f\equiv {\rm d}\ln D/{\rm d}\ln a$ is the growth rate introduced in (11); the line-of-sight component of the peculiar velocity of a given galaxy directly affect the measured redshift (hence redshift-space distortions, or RSD). Still assuming linear theory, the two-point correlation function of galaxies measured *in redshift space*, P^s, is related to the usual configuration-space power spectrum $P(k)$ via the Kaiser formula [329]

$$P^s(k,\mu) = P(k)\left[b+f\mu^2\right]^2 \tag{47}$$

where b is the bias of galaxies and μ is cosine of the angle made by wavevector $\mathbf{k}$ and the line-of-sight direction. (47) predicts the general shape of the correlation of function measured as

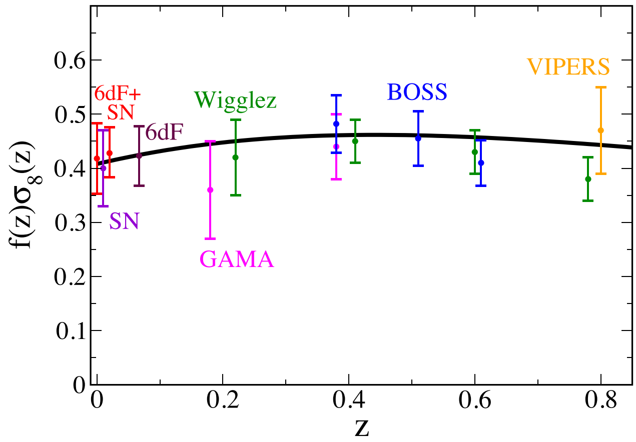

Figure 12. Constraints on the quantity $f\sigma_8$ at different redshifts from RSD and peculiar velocity surveys. At the lowest redshifts $z\approx 0$, peculiar velocities from galaxies and SNe Ia (leftmost [335] and rightmost [336] red points) and SNe Ia alone (purple data point; [337]) constrain the velocity power spectrum and effectively the quantity $f\sigma_8$. At higher redshifts, constraints on $f\sigma_8$ come from the RSD analyses from 6dFGS (maroon at $z=0.067$; [338]), GAMA (pink points; [339]), WiggleZ (dark green; [340]), BOSS (dark blue; [341]), and VIPERS (orange; [333]). The solid line shows the prediction corresponding to the currently favored flat ΛCDM cosmology.

a function of the angle between galaxy pairs and the line-of-sight. Sensitivity to dark energy mainly comes from the factor $f(a)$—more precisely, the combination $f(a)\sigma_8(a)$ [330, 331]—which is, as mentioned in section 3, very sensitive not only to dark energy parameters but also to modifications of gravity [332]. The RSD signal has been measured and used to constrain the parameter $f\sigma_8$ out to redshift $\simeq 1$, and finds good agreement with the currently favored ΛCDM model [333, 334]; see figure 12. A challenge is the theoretical modeling of the RSD; the Kaiser formula in (47) breaks down at small scales where the velocities become non-linear, requiring complex modeling combined with careful validation with numerical simulations.

6.4. Peculiar velocities

Galaxies respond to the gravitational pull of large-scale structure, leading to the so-called peculiar velocities. These motions lead to the Doppler effect: $(1+z_{\rm obs}) = (1+z)(1+v_{\parallel}/c)$, where z and $z_{\rm obs}$ are the true and observed redshift and $v_{\parallel}$ is the peculiar velocity projected along the line of sight. Roughly speaking, objects physically close to each other are being pulled by the same large-scale structures, and are therefore more likely to have similar velocities. The statistical properties of the velocity field are straightforwardly related to the matter power spectrum [342, 343]. As with the RSD, the fact that the velocity is related to density via $\nabla\cdot\mathbf{v}(\mathbf{r}) = -(aH)f\delta(\mathbf{r})$ implies that the peculiar velocities are sensitive to the quantity $f\sigma_8$, where $f\equiv{\rm d}\ln D/{\rm d}\ln a$ is the growth rate. Peculiar velocities typically determine $f\sigma_8$ at very low redshift, $z<0.1$, and thus provide an important complementary test of both dark energy and modified gravity. There has been a lot of activity in using velocities to to test for consistency with expectations from the ΛCDM model [335, 336, 344–353] and to measure cosmological parameters [337, 354]; see figure 12. Chief concerns include the reliability of distance indicators which are required in order to infer the peculiar velocity.

6.5. Hubble constant

Direct measurements of the Hubble constant offer useful complementary information that helps break degeneracy between dark energy and other cosmological parameters. This is because precise CMB measurements effectively fix high-redshift parameters including the physical matter density $\Omega_m h^2$; independent measurements of H_0 (i.e. h) therefore help determine Ω_m which is degenerate with the dark energy equation of state. Current $\gtrsim 3\sigma$ tension between the most precise direct measurements of H_0 from the Cepheid distance ladder [355, 356] and the indirect ΛCDM determination from the CMB [74] is partially, but not fully, relieved by allowing phantom dark energy ($w < -1$) or extra relativistic degrees of freedom [355]. Future measurements of the Hubble constant, expected to be at the 1% level, will not only serve as a powerful test of the ΛCDM model, but will also provide extra leverage for dark energy measurements [357].

6.6. Cosmic voids

It has been suggested that counting the cosmic voids—large underdense regions of size up to ∼100 Mpc—is an effective way to probe dark energy [358, 359]. Counting voids is similar in spirit as counting clusters of galaxies, but voids offer some advantages—they are 'more linear' than the clusters (largely thanks to the mathematical requirement that $\delta\rho/\rho \geqslant -1$), and therefore arguably more robustly modeled in numerical simulations. On the flip side, one typically uses galaxy surveys to find voids which is a challenge, given that the latter are defined as regions that are mostly devoid of galaxies. Recent work includes void catalogs extracted from the Sloan Digital Sky Survey [360–362] and even constraints on the basic ΛCDM parameters [363] but concerns remain about the robustness of the void definition in simulations, as well as their correspondence to void counts in the data [361, 364].

6.7. Shear peaks

Another method that is conceptually similar to counting clusters of galaxies is to count the peaks in the matter density field. Because the weak lensing shear is directly proportional to the matter (baryonic and dark) projected along the line of sight, counting the peaks in weak lensing maps enables this method in practice [365–370]. While primarily sensitive to the amount and distribution of matter, the method generally constrains the cosmological model, including the dark energy parameters. This probe has developed rather rapidly over the past decade, in parallel to increased quality and area of available weak lensing shear maps. Current constraints are broadly consistent with theoretical expectation the standard ΛCDM model [371–373]. The advantage of the method is that it is sensitive to non-Gaussian aspects of the lensing field, and thus provides additional information than the angular power spectrum. Principal systematics include accurately calibrating the effects of shear projection from multiple halos along the line of sight, which dominates for all except the highest peaks [369, 374] and needs to be carefully calibrated using numerical simulations [365–367, 375, 376] and measured using optimized estimators [377].

6.8. Relative ages of galaxies

If the relative ages of galaxies at different redshifts can be determined reliably, then they provide a measurement of $\mathrm{d}t/\mathrm{d}z$. Since

$$t(z) = \int_0^{t(z)} \mathrm{d}t' = \int_z^{\infty} \frac{\mathrm{d}z'}{(1+z')H(z')}\,, \tag{48}$$

one can then measure the expansion history directly [378]. Age has already been employed in cosmological constraints across a wide redshift range [379–381]. However, the presence of systematic errors due to galaxy evolution and star formation remains a serious concern.

6.9. Standard sirens

The recently detected gravitational radiation from inspiraling binary neutron stars or black holes can, in the future, enable these sources to serve as 'standard sirens' [382, 383]. From the observed waveform of each inspiral event, one can solve for the orbit's angular velocity, its rate of change, and the orbital velocity, in order to determine the luminosity of the object and hence its (absolute) luminosity distance. If the electromagnetic counterpart to the observed gravitational wave signature can be unambiguously identified, then the redshift of the host galaxy can be determined, and the inspiral can be used to probe dark energy through the Hubble diagram [384]. This potentially very complementary probe is still in the early stages of development, but holds promise to provide strong constraints on dark energy [385], out to potentially very high redshifts. Key to its success, beyond finding inspiral events at cosmological distances, is ability to localize the sources in three dimensions in order to get their redshifts [386].

6.10. Redshift drift

The redshift drift [387–389] refers to the redshift change of an object due to expansion, observed over a human timescale. The expected change of a quasar or galaxy at cosmological redshift, observed over a period of $\mathrm{d}t_0 \sim$ 10–20 years, is tiny,

$$\mathrm{d}z = [H_0(1+z) - H(z)]\,\mathrm{d}t_0 \sim 10^{-9}, \tag{49}$$

but can potentially be measured using very high-resolution spectroscopy [390]. The redshift drift method is fairly unique in its direct sensitivity to $H(z)$ across a wide redshift range and may someday contribute significantly to constraining the expansion history [391–393]. While a measurement of the redshift drift requires a very high telescope stability over a period of about a decade, there are proposals to use the intensity mapping of the 21 cm emission signal—which involves a different set of systematics—to detect the redshift-drift signal [394, 395].

6.11. Other standard candles/rulers

A wide variety of astronomical objects have been proposed as standardizable candles or rulers, useful for inferring cosmological distances via semi-empirical relations. Notable examples include radio galaxies as standardizable rulers [396, 397] and quasars as standardizable candles, most recently via the non-linear relation between UV and x-ray luminosities [398]. Long-duration gamma-ray bursts (GRBs) are an attractive possibility [399] because their ability to be detected at very high redshifts ($z \sim 6$ or higher) means they would probe a redshift range beyond that of SNe Ia. Several different relationships for GRBs have been proposed, most famously the Amati relation [400, 401] between the peak energy of the integrated spectrum and the isotropic-equivalent total energy output of the GRB. Some analyses have employed several of these relations simultaneously [402]. Due to the relatively small number of (useful) GRBs and the substantial scatter about the relations, as well as concerns about the presence of serious systematic errors, GRBs have not yielded competitive cosmological constraints. It remains to be seen whether the aforementioned relations hold over such large spans of cosmological time and can be calibrated and understood to a sufficient accuracy.

6.12. Observation of unexpected features

When interpreted in the context of a cosmological model (e.g. LCDM), observation of unexpected features in cosmological observations or existence of objects at high statistical significance can be used to rule out the model in question. High-redshift, high-mass clusters of galaxies have been particularly discussed in this context: observation of clusters had been used to disfavor the matter-only universe [28] while, more recently, there has been a discussion of whether the existence of the observed high-mass, high-redshift ‘pink elephant’ clusters are in conflict with the currently dominant LCDM paradigm (e.g. [403]). However such analyses requires a careful accounting of all sources of *statistical* error closely related to the precise way in which the observations have been carried out [404, 405]. Thus, while the observation of unexpected features can be used to rule out aspects of the dark energy paradigm, its *a posteriori* nature implies that independent confirmation that uses other cosmological probes will be required.

7. The accelerating universe: summary

In this article, we have briefly reviewed the developments leading to the discovery of dark energy and the accelerating universe. We have discussed the current status of dark energy, described parametrizations of the equation of state and physical aspects that can be measured, and reviewed both primary and secondary cosmological probes that allow us to study this mysterious component. In summary, there are a few important things to know about dark energy:

- Dark energy has negative pressure. It can be described by its present-day energy density relative to critical $\Omega_{\rm de}$ and equation of state $w \equiv p_{\rm de}/\rho_{\rm de}$. For a cosmological constant, corresponding to vacuum energy, $w = -1$ precisely and at all times. More general explanations for dark energy typically lead to a time-dependent equation of state.
- Current observational data constrain the equation of state to be $w \approx -1$ to within about 5%. Measuring w and any time dependence—as well as searching for hints of any other, as yet unseen, properties of dark energy—will help us understand the physical nature of this mysterious component, a key goal of modern cosmology.
- Dark energy is spatially smooth. It quenches the gravitational collapse of large-scale structures and suppresses the growth of density perturbations; whenever dark energy dominates, structures do not grow.
- Only relatively recently ($z \lesssim 0.5$) has dark energy come to dominate the energy budget of the universe. At earlier epochs, the dark energy density is small relative to that of matter and radiation, although a $\sim$1% contribution by dark energy at early times is still allowed by the data.
- Dark energy affects both the geometry (distances in the universe) and the growth of structure (clustering and abundance of galaxies and galaxy clusters). Separately measuring geometry and growth is an excellent way, not only to measure dark energy parameters, but also to differentiate between separate classes of dark energy models.
- Dark energy can be studied using a variety of cosmological probes that span a wide range of spatial and temporal scales and involve a wide variety of observable quantities. Control of systematic errors in these individual cosmological probes is key to their ability to discriminate testable predictions of theoretical models. The worldwide effort in theoretically modeling and observationally measuring dark energy reflects a vibrant field with many fruitful avenues that still remain to be explored.

Acknowledgments

We thank Chris Blake, Gus Evrard, Eric Linder, and Fabian Schmidt for detailed comments on earlier versions of the manuscript. DH is supported by NSF grant AST-1210974, DOE grant DEFG02-95ER40899, and NASA grant NNX16AI41G.

ORCID iDs

Dragan Huterer https://orcid.org/0000-0001-6558-0112

References

[1] Riess A G *et al* and Supernova Search Team Collaboration 1998 Observational evidence from supernovae for an accelerating universe and a cosmological constant *Astron. J.* **116** 1009–38

[2] Perlmutter S *et al* and Supernova Cosmology Project Collaboration 1999 Measurements of omega and lambda from 42 high redshift supernovae *Astrophys. J.* **517** 565–86

[3] Phillips M M 1993 The absolute magnitudes of Type Ia supernovae *Astrophys. J.* **413** L105–8

[4] Kim A G 1997 The Discovery of high redshift supernovae and their cosmological implications *PhD Thesis* UC, Berkeley

[5] Copeland E J, Sami M and Tsujikawa S 2006 Dynamics of dark energy *Int. J. Mod. Phys.* D **15** 1753–936

[6] Padmanabhan T 2003 Cosmological constant: the weight of the vacuum *Phys. Rep.* **380** 235–320

[7] Li M, Li X-D, Wang S and Wang Y 2011 Dark energy *Commun. Theor. Phys.* **56** 525–604

[8] Peebles P J E and Ratra B 2003 The cosmological constant and dark energy *Rev. Mod. Phys.* **75** 559–606

[9] Uzan J-P 2007 The acceleration of the universe and the physics behind it *Gen. Relativ. Gravit.* **39** 307–42

[10] Huterer D and Turner M S 2001 Probing the dark energy: methods and strategies *Phys. Rev.* D **64** 123527

[11] Weinberg D H, Mortonson M J, Eisenstein D J, Hirata C, Riess A G and Rozo E 2013 Observational probes of cosmic acceleration *Phys. Rep.* **530** 87–255

[12] Sahni V and Starobinsky A 2006 Reconstructing dark energy (astro-ph/0610026)

[13] Linder E V 2008 The dynamics of quintessence, the quintessence of dynamics *Gen. Relativ. Gravit.* **40** 329–56

[14] Carroll S M 2001 The cosmological constant *Living Rev. Relativ.* **4** 1

[15] Weinberg S 1989 The cosmological constant problem *Rev. Mod. Phys.* **61** 1–23

[16] Frieman J, Turner M and Huterer D 2008 Dark energy and the accelerating universe *Ann. Rev. Astron. Astrophys.* **46** 385–432

[17] Guth A H 1981 The inflationary universe: a possible solution to the horizon and flatness problems *Phys. Rev.* D **23** 347–56

[18] Linde A D 1982 A new inflationary universe scenario: a possible solution of the horizon, flatness, homogeneity, isotropy and primordial monopole problems *Phys. Lett.* B **108** 389–93

[19] Albrecht A and Steinhardt P J 1982 Cosmology for grand unified theories with radiatively induced symmetry breaking *Phys. Rev. Lett.* **48** 1220–3

[20] Fabian A C 1991 On the baryon content of the shapley supercluster *Mon. Not. R. Astron. Soc.* **253** 29P

[21] White S D M and Frenk C S 1991 Galaxy formation through hierarchical clustering *Astrophys. J.* **379** 52–79

[22] White S D M, Navarro J F, Evrard A E and Frenk C S 1993 The baryon content of galaxy clusters: a challenge to cosmological orthodoxy *Nature* **366** 429–33

[23] Maddox S J, Efstathiou G, Sutherland W J and Loveday J 1990 Galaxy correlations on large scales *Mon. Not. R. Astron. Soc.* **242** 43–9

[24] Efstathiou G, Sutherland W J and Maddox S J 1990 The cosmological constant and cold dark matter *Nature* **348** 705–7

[25] Freedman W L *et al* and Hubble Cepheid Collaboration 1994 Distance to the Virgo cluster galaxy M100 from Hubble space telescope observations of Cepheids *Nature* **371** 757–62

[26] Krauss L M and Chaboyer B 2003 Age estimates of globular clusters in the milky way: constraints on cosmology *Science* **299** 65–70

[27] Donahue M, Voit G M, Gioia I M, Luppino G, Hughes J P and Stocke J T 1998 A very hot, high redshift cluster of galaxies: more trouble for $\Omega_0 = 1$ *Astrophys. J.* **502** 550

[28] Bahcall N A and Fan X-h 1998 The most massive distant clusters: determining Ω and σ_8 *Astrophys. J.* **504** 1

[29] Scolnic D *et al* 2015 SUPERCAL: Cross=calibration of multiple photometric systems to improve cosmological measurements with type Ia supernovae *Astrophys. J.* **815** 117

[30] Alam S *et al* and BOSS Collaboration 2016 The clustering of galaxies in the completed SDSS-III baryon oscillation spectroscopic survey: cosmological analysis of the DR12 galaxy sample *Submitted to: Mon. Not. R. Astron. Soc.*

[31] Loh E D and Spillar E J 1986 A measurement of the mass density of the universe *Astrophys. J.* **307** L1

[32] Nusser A and Dekel A 1993 Omega and the initial fluctuations from velocity and density fields *Astrophys. J.* **405** 437–48

[33] Bernardeau F, Juszkiewicz R, Dekel A and Bouchet F R 1995 Omega from the skewness of the cosmic velocity divergence *Mon. Not. R. Astron. Soc.* **274** 20–6

[34] Dekel A and Rees M J 1994 Omega from velocities in voids *Astrophys. J.* **422** L1

[35] Bucher M, Goldhaber A S and Turok N 1995 An open universe from inflation *Phys. Rev.* D **52** 3314–37

[36] Ratra B and Peebles P J E 1995 Inflation in an open universe *Phys. Rev.* D **52** 1837–94

[37] Bartlett J G, Blanchard A, Silk J and Turner M S 1995 The Case for a Hubble constant of 30 $\mathrm{kms^{-1}\,Mpc^{-1}}$ *Science* **267** 980–3

[38] Perlmutter S *et al* and Supernova Cosmology Project Collaboration 1997 Measurements of the cosmological parameters Omega and Lambda from the first 7 supernovae at $z >= 0.35$ *Astrophys. J.* **483** 565

[39] Einstein A 1917 Cosmological considerations in the general theory of relativity *Sitzungsber. Preuss. Akad. Wiss. Berlin (Math. Phys.)* **1917** 142–52

[40] Peebles P J E 1984 Tests of cosmological models constrained by inflation *Astrophys. J.* **284** 439–44

[41] Turner M S, Steigman G and Krauss L M 1984 Flatness of the universe—reconciling theoretical prejudices with observational data *Phys. Rev. Lett.* **52** 2090–3

[42] Kofman L A, Gnedin N Y and Bahcall N A 1993 Cosmological constant, COBE cosmic microwave background anisotropy and large-scale clustering *Astrophys. J.* **413** 1–9

[43] Krauss L M and Turner M S 1995 The Cosmological constant is back *Gen. Relativ. Gravit.* **27** 1137–44

[44] Ostriker J P and Steinhardt P J 1995 The observational case for a low density universe with a nonzero cosmological constant *Nature* **377** 600–2

[45] Frieman J A, Hill C T, Stebbins A and Waga I 1995 Cosmology with ultralight pseudo nambu-goldstone bosons *Phys. Rev. Lett.* **75** 2077–80

[46] Stompor R, Gorski K M and Banday A J 1995 COBE—DMR normalization for inflationary flat dark matter models *Mon. Not. R. Astron. Soc.* **277** 1225

[47] Coble K, Dodelson S and Frieman J A 1997 Dynamical lambda models of structure formation *Phys. Rev.* D **55** 1851–9

[48] Liddle A R, Lyth D H, Viana P T P and White M J 1996 Cold dark matter models with a cosmological constant *Mon. Not. R. Astron. Soc.* **282** 281

[49] Perlmutter S and Schmidt B P 2003 Measuring cosmology with supernovae *Supernovae and Gamma-Ray Bursters* (*Lecture Notes in Physics* vol 598) ed K Weiler (Berlin: Springer) pp 195–217

[50] Riess A G, Press W H and Kirshner R P 1996 A precise distance indicator: Type Ia supernova multicolor light curve shapes *Astrophys. J.* **473** 88

[51] Wittman D M, Tyson J A, Bernstein G M, Lee R W, dell'Antonio I P, Fischer P, Smith D R and Blouke M M 1998 Big throughput camera: the first year *Optical Astronomical Instrumentation* (*Proc. SPIE* vol 3355) ed S D'Odorico (Bellingham, WA: SPIE) pp 626–34

[52] Rockosi C M, Gunn J E, Carr M A, Sekiguchi M, Ivezic Z and Munn J A 2002 Sloan Digital Sky Survey imaging camera: design and performance *Survey and Other Telescope Technologies and Discoveries* (*Proc. SPIE* vol 4836) ed J A Tyson and S Wolff (Bellingham, WA: SPIE) pp 180–8

[53] Miyazaki S *et al* 2002 Subaru prime focus camera: suprime-cam *Publ. Astron. Soc. Japan* **54** 833–53

[54] Kahn S M *et al* 2010 Design and development of the 3.2 gigapixel camera for the large synoptic survey telescope *Ground-based and Airborne Instrumentation for Astronomy* III (*Proc. SPIE* vol 7735) (Bellingham, WA: SPIE) p 77350J

[55] Onaka P, Rae C, Isani S, Tonry J L, Lee A, Uyeshiro R, Robertson L and Ching G 2012 GPC1 and GPC2: the Pan-STARRS 1.4 gigapixel mosaic focal plane CCD cameras with an on-sky on-CCD tip-tilt image compensation *High Energy, Optical and Infrared Detectors for Astronomy V* (*Proc. SPIE* vol 8453) (Bellingham, WA: SPIE) p 84530K

[56] McLeod B *et al* 2015 Megacam: a wide-field CCD Imager for the MMT and Magellan *Publ. Astr. Soc. Pac.* **127** 366

[57] Flaugher B *et al* and DES Collaboration 2015 The dark energy camera *Astron. J.* **150** 150

[58] Knop R A *et al* and Supernova Cosmology Project Collaboration 2003 New constraints on Omega(M), Omega(lambda) and w from an independent set of eleven high-redshift supernovae observed with HST *Astrophys. J.* **598** 102

[59] Astier P *et al* and SNLS Collaboration 2006 The Supernova legacy survey: Measurement of omega(m), omega(lambda) and W from the first year data set *Astron. Astrophys.* **447** 31–48

[60] Wood-Vasey W M *et al* and ESSENCE Collaboration 2007 Observational constraints on the nature of the dark energy: first cosmological results from the ESSENCE supernova survey *Astrophys. J.* **666** 694–715

[61] Miknaitis G *et al* 2007 The ESSENCE supernova survey: survey optimization, observations and supernova photometry *Astrophys. J.* **666** 674–93

[62] Kowalski M *et al* and Supernova Cosmology Project Collaboration 2008 Improved cosmological constraints from new, old and combined supernova datasets *Astrophys. J.* **686** 749–78

[63] Riess A G *et al* and Supernova Search Team Collaboration 2001 The farthest known supernova: support for an accelerating universe and a glimpse of the epoch of deceleration *Astrophys. J.* **560** 49–71

[64] Riess A G *et al* and Supernova Search Team Collaboration 2004 Type Ia supernova discoveries at $z > 1$ from the Hubble Space Telescope: Evidence for past deceleration and constraints on dark energy evolution *Astrophys. J.* **607** 665–87

[65] Riess A G *et al* 2007 New hubble space telescope discoveries of Type Ia supernovae at $z \geqslant 1$: narrowing constraints on the early behavior of dark energy *Astrophys. J.* **659** 98–121

[66] Huterer D and Turner M S 1999 Prospects for probing the dark energy via supernova distance measurements *Phys. Rev.* D **60** 081301

[67] Scrimgeour M *et al* 2012 The WiggleZ dark energy survey: the transition to large-scale cosmic homogeneity *Mon. Not. R. Astron. Soc.* **425** 116–34

[68] Laurent P *et al* 2016 A 14 h^{-3} Gpc^3 study of cosmic homogeneity using BOSS DR12 quasar sample *J. Cosmol. Astropart. Phys.* JCAP11(2016)060

[69] Peebles P J E 1980 The large-scale structure of the universe

[70] Linder E V 2005 Cosmic growth history and expansion history *Phys. Rev.* D **72** 043529

[71] Linder E V and Cahn R N 2007 Parameterized beyond-Einstein growth *Astropart. Phys.* **28** 481–8

[72] Takahashi R, Sato M, Nishimichi T, Taruya A and Oguri M 2012 Revising the Halofit model for the nonlinear matter power spectrum *Astrophys. J.* **761** 152

[73] Mead A, Heymans C, Lombriser L, Peacock J, Steele O and Winther H 2016 Accurate halo-model matter power spectra with dark energy, massive neutrinos and modified gravitational forces *Mon. Not. R. Astron. Soc.* **459** 1468–88

[74] Ade P A R *et al* and Planck Collaboration 2016 Planck 2015 results. XIII. Cosmological parameters *Astron. Astrophys.* **594** A13

[75] Linder E V 1988 Cosmological tests of generalized Friedmann models *Astron. Astrophys.* **206** 175–89

[76] Turner M S and White M J 1997 Cdm models with a smooth component *Phys. Rev.* D **56** 4439–43

[77] Cooray A R and Huterer D 1999 Gravitational lensing as a probe of quintessence *Astrophys. J.* **513** L95–8

[78] Gerke B F and Efstathiou G 2002 Probing quintessence: Reconstruction and parameter estimation from supernovae *Mon. Not. R. Astron. Soc.* **335** 33

[79] Linder E V 2003 Exploring the expansion history of the universe *Phys. Rev. Lett.* **90** 091301

[80] Chevallier M and Polarski D 2001 Accelerating universes with scaling dark matter *Int. J. Mod. Phys.* D **10** 213–24

[81] Sahni V, Saini T D, Starobinsky A A and Alam U 2003 Statefinder: a new geometrical diagnostic of dark energy *JETP Lett.* **77** 201–6
Sahni V, Saini T D, Starobinsky A A and Alam U 2003 *Pisma Zh. Eksp. Teor. Fiz.* **77** 249

[82] Corasaniti P S, Kunz M, Parkinson D, Copeland E J and Bassett B A 2004 The foundations of observing dark energy dynamics with the wilkinson microwave anisotropy probe *Phys. Rev.* D **70** 083006

[83] Huterer D and Starkman G 2003 Parameterization of dark-energy properties: a principal- component approach *Phys. Rev. Lett.* **90** 031301

[84] Albrecht A *et al* 2009 Findings of the joint dark energy mission figure of merit science working group (arXiv:0901.0721)

[85] Ruiz E J, Shafer D L, Huterer D and Conley A 2012 Principal components of dark energy with SNLS supernovae: the effects of systematic errors *Phys. Rev.* D **86** 103004

[86] Mortonson M J, Hu W and Huterer D 2009 Falsifying paradigms for cosmic acceleration *Phys. Rev.* D **79** 023004

[87] de Putter R and Linder E V 2008 To bin or not to bin: decorrelating the cosmic equation of state *Astropart. Phys.* **29** 424

[88] Huterer D and Cooray A 2005 Uncorrelated estimates of dark energy evolution *Phys. Rev.* D **71** 023506

[89] Hu W 2002 Dark energy and matter evolution from lensing tomography *Phys. Rev.* D **66** 083515

[90] Hojjati A, Zhao G-B, Pogosian L, Silvestri A, Crittenden R and Koyama K 2012 Cosmological tests of general relativity: a principal component analysis *Phys. Rev.* D **85** 043508

[91] Zhao G-B, Pogosian L, Silvestri A and Zylberberg J 2009 Cosmological tests of general relativity with future tomographic surveys *Phys. Rev. Lett.* **103** 241301

[92] Ade P A R *et al* and Planck Collaboration 2016 Planck 2015 results. XIV. Dark energy and modified gravity *Astron. Astrophys.* **594** A14

[93] Saini T D, Raychaudhury S, Sahni V and Starobinsky A A 2000 Reconstructing the cosmic equation of state from supernova distances *Phys. Rev. Lett.* **85** 1162–5

[94] Nakamura T and Chiba T 1999 Determining the equation of state of the expanding universe: inverse problem in cosmology *Mon. Not. R. Astron. Soc.* **306** 696–700

[95] Starobinsky A A 1998 How to determine an effective potential for a variable cosmological term *JETP Lett.* **68** 757–63

[96] Wang Y and Mukherjee P 2004 Model-independent constraints on dark energy density from flux-averaging analysis of type ia supernova data *Astrophys. J.* **606** 654–63

[97] Wang Y and Tegmark M 2005 Uncorrelated measurements of the cosmic expansion history and dark energy from supernovae *Phys. Rev.* D **71** 103513

[98] Weller J and Albrecht A 2002 Future supernovae observations as a probe of dark energy *Phys. Rev.* D **65** 103512

[99] Holsclaw T, Alam U, Sanso B, Lee H, Heitmann K, Habib S and Higdon D 2010 Nonparametric dark energy reconstruction from supernova data *Phys. Rev. Lett.* **105** 241302

[100] Crittenden R G, Zhao G-B, Pogosian L, Samushia L and Zhang X 2012 Fables of reconstruction: controlling bias in the dark energy equation of state *J. Cosmol. Astropart. Phys.* JCAP02(2012)048

[101] Shafieloo A, Kim A G and Linder E V 2012 Gaussian process cosmography *Phys. Rev.* D **85** 123530

[102] Zhao G-B, Crittenden R G, Pogosian L and Zhang X 2012 Examining the evidence for dynamical dark energy *Phys. Rev. Lett.* **109** 171301

[103] Shafieloo A, Kim A G and Linder E V 2013 Model independent tests of cosmic growth versus expansion *Phys. Rev.* D **87** 023520

[104] Albrecht A *et al* 2006 Report of the dark energy task force (astro-ph/0609591)

[105] Mortonson M J, Huterer D and Hu W 2010 Figures of merit for present and future dark energy probes *Phys. Rev.* D **82** 063004

[106] Hu W 1998 Structure formation with generalized dark matter *Astrophys. J.* **506** 485–94

[107] Hu W and Eisenstein D J 1999 The structure of structure formation theories *Phys. Rev.* D **59** 083509

[108] Erickson J K, Caldwell R R, Steinhardt P J, Armendariz-Picon C and Mukhanov V F 2002 Measuring the speed of sound of quintessence *Phys. Rev. Lett.* **88** 121301

[109] DeDeo S, Caldwell R R and Steinhardt P J 2003 Effects of the sound speed of quintessence on the microwave background and large scale structure *Phys. Rev.* D **67** 103509
DeDeo S, Caldwell R R and Steinhardt P J 2004 *Phys. Rev.* D **69** 129902 (erratum)

[110] Weller J and Lewis A M 2003 Large scale cosmic microwave background anisotropies and dark energy *Mon. Not. R. Astron. Soc.* **346** 987–93

[111] Hannestad S 2005 Constraints on the sound speed of dark energy *Phys. Rev.* D **71** 103519

[112] de Putter R, Huterer D and Linder E V 2010 Measuring the speed of dark: detecting dark energy perturbations *Phys. Rev.* D **81** 103513

[113] Wetterich C 2004 Phenomenological parameterization of quintessence *Phys. Lett.* B **594** 17–22

[114] Doran M and Robbers G 2006 Early dark energy cosmologies *J. Cosmol. Astropart. Phys.* JCAP06(2006)026

[115] Linder E V 2006 Dark energy in the dark ages *Astropart. Phys.* **26** 16–21

[116] Zlatev I, Wang L-M and Steinhardt P J 1999 Quintessence, cosmic coincidence and the cosmological constant *Phys. Rev. Lett.* **82** 896–9

[117] Linder E V and Smith T L 2011 Dark before light: testing the cosmic expansion history through the cosmic microwave background *J. Cosmol. Astropart. Phys.* JCAP04(2011)001

[118] Reichardt C L, de Putter R, Zahn O and Hou Z 2012 New limits on early dark energy from the south pole telescope *Astrophys. J.* **749** L9

[119] Calabrese E, Huterer D, Linder E V, Melchiorri A and Pagano L 2011 Limits on dark radiation, early dark energy and relativistic degrees of freedom *Phys. Rev.* D **83** 123504

[120] Gradwohl B-A and Frieman J A 1992 Dark matter, long range forces and large scale structure *Astrophys. J.* **398** 407–24

[121] Amendola L 2000 Coupled quintessence *Phys. Rev.* D **62** 043511

[122] Farrar G R and Peebles P J E 2004 Interacting dark matter and dark energy *Astrophys. J.* **604** 1–11

[123] Wang B, Abdalla E, Atrio-Barandela F and Pavon D 2016 Dark matter and dark energy interactions: theoretical challenges, cosmological implications and observational signatures *Rep. Prog. Phys.* **79** 096901

[124] Silvestri A and Trodden M 2009 Approaches to understanding cosmic acceleration *Rep. Prog. Phys.* **72** 096901

[125] Joyce A, Jain B, Khoury J and Trodden M 2015 Beyond the cosmological standard model *Phys. Rep.* **568** 1–98

[126] Joyce A, Lombriser L and Schmidt F 2016 Dark energy versus modified gravity *Ann. Rev. Nucl. Part. Sci.* **66** 95–122

[127] Daniel S F and Linder E V 2013 Constraining cosmic expansion and gravity with galaxy redshift surveys *J. Cosmol. Astropart. Phys.* JCAP02(2013)007

[128] Caldwell R, Cooray A and Melchiorri A 2007 Constraints on a new post-general relativity cosmological parameter *Phys. Rev.* D **76** 023507

[129] Bertschinger E and Zukin P 2008 Distinguishing modified gravity from dark energy *Phys. Rev.* D **78** 024015

[130] Daniel S F, Linder E V, Smith T L, Caldwell R R, Cooray A, Leauthaud A and Lombriser L 2010 Testing general relativity with current cosmological data *Phys. Rev.* D **81** 123508

[131] Asaba S *et al* 2013 Principal component analysis of modified gravity using weak lensing and peculiar velocity measurements *J. Cosmol. Astropart. Phys.* JCAP08(2013)029

[132] Bean R and Tangmatitham M 2010 Current constraints on the cosmic growth history *Phys. Rev.* D **81** 083534

[133] Zhao G-B *et al* 2012 Testing Einstein gravity with cosmic growth and expansion *Phys. Rev.* D **85** 123546

[134] Dossett J N, Ishak M and Moldenhauer J 2011 Testing general relativity at cosmological scales: implementation and parameter correlations *Phys. Rev.* D **84** 123001

[135] Silvestri A, Pogosian L and Buniy R V 2013 Practical approach to cosmological perturbations in modified gravity *Phys. Rev.* D **87** 104015

[136] Huterer D and Linder E V 2007 Separating dark physics from physical darkness: minimalist modified gravity versus dark energy *Phys. Rev.* D **75** 023519

[137] Zhang P, Liguori M, Bean R and Dodelson S 2007 Probing gravity at cosmological scales by measurements which test the relationship between gravitational lensing and matter overdensity *Phys. Rev. Lett.* **99** 141302

[138] Reyes R, Mandelbaum R, Seljak U, Baldauf T, Gunn J E, Lombriser L and Smith R E 2010 Confirmation of general relativity on large scales from weak lensing and galaxy velocities *Nature* **464** 256–8
[139] Marshall P, Rajguru N and Slosar A 2006 Bayesian evidence as a tool for comparing datasets *Phys. Rev.* D **73** 067302
[140] Trotta R 2008 Bayes in the sky: Bayesian inference and model selection in cosmology *Contemp. Phys.* **49** 71–104
[141] Grandis S, Seehars S, Refregier A, Amara A and Nicola A 2016 Information gains from cosmological probes *J. Cosmol. Astropart. Phys.* JCAP05(2016)034
[142] Raveri M 2016 Are cosmological data sets consistent with each other within the Λ cold dark matter model? *Phys. Rev.* D **93** 043522
[143] Charnock T, Battye R A and Moss A 2017 Planck data versus large scale structure *Phys. Rev.* D **95** 123535
[144] Lin W and Ishak M 2017 Cosmological discordances: a new measure, marginalization effects and application to geometry versus growth current data sets *Phys. Rev.* D **96** 023532
[145] Lin W and Ishak M 2017 Cosmological discordances II: Hubble constant, Planck and large-scale-structure data sets *Phys. Rev.* D **96** 083532
[146] Mortonson M J, Hu W and Huterer D 2010 Testable dark energy predictions from current data *Phys. Rev.* D **81** 063007
[147] Vanderveld R A, Mortonson M J, Hu W and Eifler T 2012 Testing dark energy paradigms with weak gravitational lensing *Phys. Rev.* D **85** 103518
[148] Ishak M, Upadhye A and Spergel D N 2006 Probing cosmic acceleration beyond the equation of state: distinguishing between dark energy and modified gravity models *Phys. Rev.* D **74** 043513
[149] Wang S, Hui L, May M and Haiman Z 2007 Is modified gravity required by observations? An empirical consistency test of dark energy models *Phys. Rev.* D **76** 063503
[150] Zhang J, Hui L and Stebbins A 2005 Isolating geometry in weak lensing measurements *Astrophys. J.* **635** 806–20
[151] MacCrann N, Zuntz J, Bridle S, Jain B and Becker M R 2015 Cosmic discordance: are Planck CMB and CFHTLenS weak lensing measurements out of tune? *Mon. Not. R. Astron. Soc.* **451** 2877–88
[152] Ruiz E J and Huterer D 2015 Testing the dark energy consistency with geometry and growth *Phys. Rev.* D **91** 063009
[153] Bernal J L, Verde L and Cuesta A J 2016 Parameter splitting in dark energy: is dark energy the same in the background and in the cosmic structures? *J. Cosmol. Astropart. Phys.* JCAP02(2016)059
[154] Kowal C T 1968 Absolute magnitudes of supernovae *Astron. J.* **73** 1021–4
[155] Maoz D and Mannucci F 2012 Type-Ia supernova rates and the progenitor problem, a review *Publ. Astron. Soc. Austral.* **29** 447
[156] Wang B and Han Z 2012 Progenitors of type Ia supernovae *New Astron. Rev.* **56** 122–41
[157] Baade W and Zwicky F 1934 On Super-novae *Proc. Natl Acad. Sci.* **20** 254–9
[158] Wagoner R V 1977 Determining q0 from Supernovae *Astrophys. J.* **214** L5+
[159] Colgate S A 1979 Supernovae as a standard candle for cosmology *Astrophys. J.* **232** 404–8
[160] Norgaard-Nielsen H U, Hansen L, Jorgensen H E, Aragon Salamanca A and Ellis R S 1989 The discovery of a type IA supernova at a redshift of 0.31 *Nature* **339** 523–5
[161] Guy J *et al* and SNLS Collaboration 2007 SALT2: using distant supernovae to improve the use of Type Ia supernovae as distance indicators *Astron. Astrophys.* **466** 11–21
[162] Hicken M *et al* 2009 Improved dark energy constraints from 100 new CfA supernova Type Ia light curves *Astrophys. J.* **700** 1097–140
[163] Amanullah R *et al* 2010 Spectra and light curves of six Type Ia supernovae at $0.511 < z < 1.12$ and the Union2 compilation *Astrophys. J.* **716** 712–38
[164] Conley A *et al* and SNLS Collaboration 2011 Supernova constraints and systematic uncertainties from the first 3 years of the supernova legacy survey *Astrophys. J. Suppl.* **192** 1
[165] Holz D E and Linder E V 2005 Safety in numbers: gravitational lensing degradation of the luminosity distance-redshift relation *Astrophys. J.* **631** 678–88
[166] March M C, Trotta R, Berkes P, Starkman G D and Vaudrevange P M 2011 Improved constraints on cosmological parameters from SNIa data *Mon. Not. R. Astron. Soc.* **418** 2308–29
March M C, Trotta R, Berkes P, Starkman G D and Vaudrevange P M 2011 *Mon. Not. R. Astron. Soc.* **418** 4
[167] Rubin D *et al* and Supernova Cosmology Project Collaboration 2015 Unity: confronting supernova cosmology's statistical and systematic uncertainties in a unified Bayesian framework *Astrophys. J.* **813** 137
[168] Kunz M, Bassett B A and Hlozek R 2007 Bayesian estimation applied to multiple species: towards cosmology with a million supernovae *Phys. Rev.* D **75** 103508
[169] Hlozek R *et al* 2012 Photometric supernova cosmology with BEAMS and SDSS-II *Astrophys. J.* **752** 79
[170] Jones D O *et al* 2017 Measuring the properties of dark energy with photometrically classified Pan-STARRS Supernovae. I. Systematic uncertainty from core-collapse supernova contamination *Astrophys. J.* **843** 6
[171] Scolnic D and Kessler R 2016 Measuring Type Ia supernova populations of stretch and color and predicting distance biases *Astrophys. J.* **822** L35
[172] Kessler R and Scolnic D 2017 Correcting Type Ia supernova distances for selection biases and contamination in photometrically identified samples *Astrophys. J.* **836** 56
[173] Foley R J and Kirshner R P 2013 Metallicity differences in Type Ia supernova progenitors inferred from ultraviolet spectra *Astrophys. J.* **769** L1
[174] Graham M L, Foley R J, Zheng W, Kelly P L, Shivvers I, Silverman J M, Filippenko A V, Clubb K I and Ganeshalingam M 2015 Twins for life? A comparative analysis of the Type Ia supernovae 2011fe and 2011by *Mon. Not. R. Astron. Soc.* **446** 2073–88
[175] Milne P A, Foley R J, Brown P J and Narayan G 2015 The changing fractions of Type ia supernova Nuv-optical subclasses with redshift *Astrophys. J.* **803** 20
[176] Fakhouri H K *et al* and Nearby Supernova Factory Collaboration 2015 Improving cosmological distance measurements using twin Type Ia supernovae *Astrophys. J.* **815** 58
[177] Sunyaev R A and Zeldovich Ya B 1970 Small scale fluctuations of relic radiation *Astrophys. Space Sci.* **7** 3–19
[178] Peebles P J E and Yu J T 1970 Primeval adiabatic perturbation in an expanding universe *Astrophys. J.* **162** 815–36
[179] Eisenstein D J *et al* and SDSS Collaboration 2005 Detection of the baryon acoustic peak in the large-scale correlation function of SDSS luminous red galaxies *Astrophys. J.* **633** 560–74
[180] Cole S *et al* and 2dFGRS Collaboration 2005 The 2dF galaxy redshift survey: power-spectrum analysis of the final dataset and cosmological implications *Mon. Not. R. Astron. Soc.* **362** 505–34

[181] Padmanabhan N *et al* and SDSS Collaboration 2007 The clustering of luminous red galaxies in the sloan digital sky survey imaging data *Mon. Not. R. Astron. Soc.* **378** 852–72

[182] Percival W J, Cole S, Eisenstein D J, Nichol R C, Peacock J A, Pope A C and Szalay A S 2007 Measuring the baryon acoustic oscillation scale using the SDSS and 2dFGRS *Mon. Not. R. Astron. Soc.* **381** 1053–66

[183] Blake C *et al* 2011 The WiggleZ dark energy survey: mapping the distance-redshift relation with baryon acoustic oscillations *Mon. Not. R. Astron. Soc.* **418** 1707–24

[184] Beutler F, Blake C, Colless M, Jones D H, Staveley-Smith L, Campbell L, Parker Q, Saunders W and Watson F 2011 The 6dF galaxy survey: baryon acoustic oscillations and the local hubble constant *Mon. Not. R. Astron. Soc.* **416** 3017–32

[185] Padmanabhan N, Xu X, Eisenstein D J, Scalzo R, Cuesta A J, Mehta K T and Kazin E 2012 A 2 per cent distance to $z = 0.35$ by reconstructing baryon acoustic oscillations—I. Methods and application to the sloan digital sky survey *Mon. Not. R. Astron. Soc.* **427** 2132–45

[186] Anderson L *et al* and BOSS Collaboration 2014 The clustering of galaxies in the SDSS-III baryon oscillation spectroscopic survey: baryon acoustic oscillations in the data releases 10 and 11 Galaxy samples *Mon. Not. R. Astron. Soc.* **441** 24–62

[187] Ross A J, Samushia L, Howlett C, Percival W J, Burden A and Manera M 2015 The clustering of the SDSS DR7 main Galaxy sample—I. A 4 per cent distance measure at $z = 0.15$ *Mon. Not. R. Astron. Soc.* **449** 835–47

[188] Blake C and Glazebrook K 2003 Probing dark energy using baryonic oscillations in the galaxy power spectrum as a cosmological ruler *Astrophys. J.* **594** 665–73

[189] Hu W and Haiman Z 2003 Redshifting rings of power *Phys. Rev.* D **68** 063004

[190] Seo H-J and Eisenstein D J 2003 Probing dark energy with baryonic acoustic oscillations from future large galaxy redshift surveys *Astrophys. J.* **598** 720–40

[191] Padmanabhan N and White M 2009 Calibrating the baryon oscillation ruler for matter and halos *Phys. Rev.* D **80** 063508

[192] Mehta K T, Seo H-J, Eckel J, Eisenstein D J, Metchnik M, Pinto P and Xu X 2011 Galaxy bias and its effects on the baryon acoustic oscillations measurements *Astrophys. J.* **734** 94

[193] Seo H-J, Eckel J, Eisenstein D J, Mehta K, Metchnik M, Padmanabhan N, Pinto P, Takahashi R, White M and Xu X 2010 High-precision predictions for the acoustic scale in the non-linear regime *Astrophys. J.* **720** 1650–67

[194] Desjacques V, Jeong D and Schmidt F 2016 Large-scale galaxy bias (arXiv:1611.09787)

[195] Ellis R *et al* and PFS Team Collaboration 2014 Extragalactic science, cosmology and galactic archaeology with the Subaru prime focus spectrograph *Publ. Astron. Soc. Japan* **66** R1

[196] Aghamousa A *et al* and DESI Collaboration 2016 The DESI experiment part I: science,targeting and survey design (arXiv:1611.00036)

[197] Aghamousa A *et al* and DESI Collaboration 2016 The DESI experiment part II: instrument design (arXiv:1611.00037)

[198] Busca N G *et al* 2013 Baryon acoustic oscillations in the Ly-α forest of BOSS quasars *Astron. Astrophys.* **552** A96

[199] Slosar A *et al* 2013 Measurement of baryon acoustic oscillations in the lyman-alpha forest fluctuations in BOSS Data release 9 *J. Cosmol. Astropart. Phys.* JCAP04(2013)026

[200] Font-Ribera A *et al* and BOSS Collaboration 2014 Quasar-lyman α forest cross-correlation from BOSS DR11: baryon acoustic oscillations *J. Cosmol. Astropart. Phys.* JCAP05(2014)027

[201] Delubac T *et al* and BOSS Collaboration 2015 Baryon acoustic oscillations in the Ly forest of BOSS DR11 quasars *Astron. Astrophys.* **574** A59

[202] Bautista J E *et al* 2017 Measurement of baryon acoustic oscillation correlations at $z = 2.3$ with SDSS DR12 Lyα-Forests *Astron. Astrophys.* **603** A12

[203] Betoule M *et al* and SDSS Collaboration 2014 Improved cosmological constraints from a joint analysis of the SDSS-II and SNLS supernova samples *Astron. Astrophys.* **568** A22

[204] Bennett C L, Turner M S and White M 1997 The cosmic Rosetta stone *Phys. Today* **50** 32–8

[205] Hu W and Dodelson S 2002 Cosmic microwave background anisotropies *Ann. Rev. Astron. Astrophys.* **40** 171–216

[206] Bond J R, Efstathiou G and Tegmark M 1997 Forecasting cosmic parameter errors from microwave background anisotropy experiments *Mon. Not. R. Astron. Soc.* **291** L33–41

[207] Melchiorri A, Mersini-Houghton L, Odman C J and Trodden M 2003 The State of the dark energy equation of state *Phys. Rev.* D **68** 043509

[208] Frieman J A, Huterer D, Linder E V and Turner M S 2003 Probing dark energy with supernovae: exploiting complementarity with the cosmic microwave background *Phys. Rev.* D **67** 083505

[209] Sherwin B D *et al* 2011 Evidence for dark energy from the cosmic microwave background alone using the Atacama cosmology telescope lensing measurements *Phys. Rev. Lett.* **107** 021302

[210] Jaffe A H *et al* and Boomerang Collaboration 2001 Cosmology from MAXIMA-1, BOOMERANG and COBE / DMR CMB observations *Phys. Rev. Lett.* **86** 3475–9

[211] Sievers J L *et al* 2003 Cosmological parameters from cosmic background imager observations and comparisons with BOOMERANG, DASI and MAXIMA *Astrophys. J.* **591** 599–622

[212] Spergel D N *et al* and WMAP Collaboration 2003 First year wilkinson microwave anisotropy probe (wmap) observations: Determination of cosmological parameters *Astrophys. J. Suppl.* **148** 175

[213] Spergel D N *et al* 2007 Three-year Wilkinson microwave anisotropy probe (WMAP) observations: implications for cosmology *Astrophys. J. Suppl.* **170** 377–408

[214] Komatsu E *et al* and WMAP Collaboration 2009 Five-year Wilkinson microwave anisotropy probe (WMAP) observations: cosmological interpretation *Astrophys. J. Suppl.* **180** 330–76

[215] Komatsu E *et al* and WMAP Collaboration 2011 Seven-Year Wilkinson microwave anisotropy probe (WMAP) observations: cosmological interpretation *Astrophys. J. Suppl.* **192** 18

[216] Hinshaw G *et al* and WMAP Collaboration 2013 Nine-Year Wilkinson microwave anisotropy probe (WMAP) observations: cosmological interpretation *Astrophys. J. Suppl.* **208** 19

[217] Ade P A R *et al* and Planck Collaboration 2014 Planck 2013 results. XVI. Cosmological parameters *Astron. Astrophys.* **571** A16

[218] Hou Z *et al* 2014 Constraints on Cosmology from the Cosmic Microwave Background Power Spectrum of the 2500 deg^2 SPT-SZ Survey *Astrophys. J.* **782** 74

[219] Sievers J L *et al* and Atacama Cosmology Telescope Collaboration 2013 The Atacama cosmology telescope: cosmological parameters from three seasons of data *J. Cosmol. Astropart. Phys.* JCAP10(2013)060

[220] Sachs R K and Wolfe A M 1967 Perturbations of a cosmological model and angular variations of the microwave background *Astrophys. J.* **147** 73–90
Sachs R K and Wolfe A M 2007 *Gen. Relativ. Gravit.* **39** 1929
[221] Hu W and Sugiyama N 1994 The small scale integrated Sachs–Wolfe effect *Phys. Rev.* D **50** 627–31
[222] Hu W 2002 Dark synergy: gravitational lensing and the CMB *Phys. Rev.* D **65** 023003
[223] Bean R and Dore O 2004 Probing dark energy perturbations: the dark energy equation of state and speed of sound as measured by WMAP *Phys. Rev.* D **69** 083503
[224] Song Y-S, Sawicki I and Hu W 2007 Large-scale tests of the DGP model *Phys. Rev.* D **75** 064003
[225] Bartelmann M and Schneider P 2001 Weak gravitational lensing *Phys. Rep.* **340** 291–472
[226] Hoekstra H and Jain B 2008 Weak gravitational lensing and its cosmological applications *Ann. Rev. Nucl. Part. Sci.* **58** 99–123
[227] Huterer D 2010 Weak lensing, dark matter and dark energy *Gen. Relativ. Gravit.* **42** 2177–95
[228] Takada M and Jain B 2004 Cosmological parameters from lensing power spectrum and bispectrum tomography *Mon. Not. R. Astron. Soc.* **348** 897
[229] Hu W 1999 Power spectrum tomography with weak lensing *Astrophys. J.* **522** L21–4
[230] Jarvis M, Jain B, Bernstein G and Dolney D 2006 Dark energy constraints from the CTIO lensing survey *Astrophys. J.* **644** 71–9
[231] Massey R *et al* 2007 COSMOS: 3D weak lensing and the growth of structure *Astrophys. J. Suppl.* **172** 239–53
[232] Schrabback T *et al* 2010 Evidence for the accelerated expansion of the Universe from weak lensing tomography with COSMOS *Astron. Astrophys.* **516** A63
[233] Lin H, Dodelson S, Seo H-J, Soares-Santos M, Annis J, Hao J, Johnston D, Kubo J M, Reis R R R and Simet M and SDSS Collaboration 2012 The SDSS Coadd: cosmic shear measurement *Astrophys. J.* **761** 15
[234] Heymans C *et al* 2013 CFHTLenS tomographic weak lensing cosmological parameter constraints: mitigating the impact of intrinsic galaxy alignments *Mon. Not. R. Astron. Soc.* **432** 2433
[235] Huff E M, Eifler T, Hirata C M, Mandelbaum R, Schlegel D and Seljak U 2014 Seeing in the dark. 2. Cosmic shear in the sloan digital sky survey *Mon. Not. R. Astron. Soc.* **440** 1322–44
[236] Jee M J, Tyson J A, Hilbert S, Schneider M D, Schmidt S and Wittman D 2016 Cosmic shear results from the deep lens survey—II: full cosmological parameter constraints from tomography *Astrophys. J.* **824** 77
[237] Hildebrandt H *et al* 2017 KiDS-450: cosmological parameter constraints from tomographic weak gravitational lensing *Mon. Not. R. Astron. Soc.* **465** 1454
[238] Troxel M A *et al* and DES Collaboration 2017 Dark energy survey year 1 results: cosmological constraints from cosmic shear (arXiv:1708.01538)
[239] Huterer D, Takada M, Bernstein G and Jain B 2006 Systematic errors in future weak lensing surveys: requirements and prospects for self-calibration *Mon. Not. R. Astron. Soc.* **366** 101–14
[240] Heymans C, White M, Heavens A, Vale C and van Waerbeke L 2006 Potential sources of contamination to weak lensing measurements: constraints from N-body simulations *Mon. Not. R. Astron. Soc.* **371** 750–60
[241] Mandelbaum R *et al* 2014 The third gravitational lensing accuracy testing (GREAT3) challenge handbook *Astrophys. J. Suppl.* **212** 5
[242] Ma Z-M, Hu W and Huterer D 2005 Effect of photometric redshift uncertainties on weak lensing tomography *Astrophys. J.* **636** 21–9
[243] Hearin A P, Zentner A R, Ma Z and Huterer D 2010 A general study of the influence of catastrophic photometric redshift errors on cosmology with cosmic shear tomography *Astrophys. J.* **720** 1351–69
[244] Huterer D and Takada M 2005 Calibrating the nonlinear matter power spectrum: requirements for future weak lensing surveys *Astropart. Phys.* **23** 369–76
[245] Rudd D H, Zentner A R and Kravtsov A V 2008 Effects of baryons and dissipation on the matter power spectrum *Astrophys. J.* **672** 19–32
[246] Hearin A P and Zentner A R 2009 The influence of galaxy formation physics on weak lensing tests of general relativity *J. Cosmol. Astropart. Phys.* JCAP04(2009)032
[247] Takada M and Jain B 2009 The impact of non-Gaussian errors on weak lensing surveys *Mon. Not. R. Astron. Soc.* **395** 2065–86
[248] Taylor A, Joachimi B and Kitching T 2013 Putting the precision in precision cosmology: how accurate should your data covariance matrix be? *Mon. Not. R. Astron. Soc.* **432** 1928
[249] Dodelson S and Schneider M D 2013 The effect of covariance estimator error on cosmological parameter constraints *Phys. Rev.* D **88** 063537
[250] Joachimi B *et al* 2015 Galaxy alignments: an overview *Space Sci. Rev.* **193** 1–65
[251] Abbott T M C *et al* and DES Collaboration 2017 Dark energy survey year 1 results: cosmological constraints from galaxy clustering and weak lensing (arXiv:1708.01530)
[252] Aihara H *et al* 2017 First data release of the hyper suprime-cam subaru strategic program (arXiv:1702.08449)
[253] Cai Y-C and Bernstein G 2012 Combining weak lensing tomography and spectroscopic redshift surveys *Mon. Not. R. Astron. Soc.* **422** 1045–56
[254] Joachimi B, Mandelbaum R, Abdalla F B and Bridle S L 2011 Constraints on intrinsic alignment contamination of weak lensing surveys using the MegaZ-LRG sample *Astron. Astrophys.* **527** A26
[255] Font-Ribera A, McDonald P, Mostek N, Reid B A, Seo H-J and Slosar A 2014 DESI and other dark energy experiments in the era of neutrino mass measurements *J. Cosmol. Astropart. Phys.* JCAP05(2014)023
[256] Eriksen M and Gaztanaga E 2015 Combining spectroscopic and photometric surveys: same or different sky? *Mon. Not. R. Astron. Soc.* **451** 1553–60
[257] van Uitert E *et al* 2017 KiDS+ GAMA: Cosmology constraints from a joint analysis of cosmic shear, galaxy–galaxy lensing and angular clustering (arXiv:1706.05004)
[258] Joudaki S *et al* 2017 KiDS-450 + 2dFLenS: Cosmological parameter constraints from weak gravitational lensing tomography and overlapping redshift-space galaxy clustering (arXiv:1707.06627)
[259] Wittman D, Tyson J A, Margoniner V E, Cohen J G and Dell'Antonio I P 2001 Discovery of a Galaxy cluster via weak lensing *Astrophys. J.* **557** L89–92
[260] Wittman D, Margoniner V E, Tyson J A, Cohen J G and Dell'Antonio I P 2003 Weak lensing discovery and tomography of a cluster at $z = 0.68$ *Astrophys. J.* **597** 218–24
[261] Wittman D *et al* 2006 First results on shear-selected clusters from the deep lens survey: optical imaging, spectroscopy and x-ray followup *Astrophys. J.* **643** 128
[262] Schirmer M, Erben T, Hetterscheidt M and Schneider P 2007 GaBoDS: the Garching–Bonn deep survey. IX. A sample of 158 shear-selected mass concentration candidates *Astron. Astrophys.* **462** 875–87

[263] Dietrich J P, Erben T, Lamer G, Schneider P, Schwope A, Hartlap J and Maturi M 2007 BLOX: the Bonn lensing, optical and x-ray selected galaxy clusters. I. Cluster catalog construction *Astron. Astrophys.* **470** 821–34

[264] Miyazaki S, Hamana T, Ellis R S, Kashikawa N, Massey R J, Taylor J and Refregier A 2007 A subaru weak-lensing survey. I. Cluster candidates and spectroscopic verification *Astrophys. J.* **669** 714–28

[265] Clowe D *et al* 2006 A direct empirical proof of the existence of dark matter *Astrophys. J.* **648** L109–13

[266] Allen S W, Evrard A E and Mantz A B 2011 Cosmological parameters from observations of galaxy clusters *Ann. Rev. Astron. Astrophys.* **49** 409–70

[267] Heitmann K *et al* 2016 The Mira-Titan Universe: precision predictions for dark energy surveys *Astrophys. J.* **820** 108

[268] Press W H and Schechter P 1974 Formation of galaxies and clusters of galaxies by selfsimilar gravitational condensation *Astrophys. J.* **187** 425–38

[269] Gunn J E and Gott J R III 1972 On the infall of matter into clusters of galaxies and some effects on their evolution *Astrophys. J.* **176** 1–19

[270] Zentner A R 2007 The excursion set theory of halo mass functions, halo clustering and halo growth *Int. J. Mod. Phys.* D **16** 763–816

[271] Tinker J L *et al* 2008 Toward a halo mass function for precision cosmology: the limits of universality *Astrophys. J.* **688** 709–28

[272] Linder E V and Jenkins A 2003 Cosmic structure and dark energy *Mon. Not. R. Astron. Soc.* **346** 573

[273] Baldi M 2012 Dark energy simulations *Phys. Dark Univ.* **1** 162–93

[274] Vikhlinin A *et al* 2009 Chandra cluster cosmology project III: cosmological parameter constraints *Astrophys. J.* **692** 1060–74

[275] Evrard A E, Arnault P, Huterer D and Farahi A 2014 A model for multiproperty galaxy cluster statistics *Mon. Not. R. Astron. Soc.* **441** 3562–9

[276] Rykoff E S, Koester B P, Rozo E, Annis J, Evrard A E, Hansen S M, Hao J, Johnston D E, McKay T A and Wechsler R H 2012 Robust optical richness estimation with reduced scatter *Astrophys. J.* **746** 178

[277] Rykoff E S *et al* 2014 redMaPPer I: algorithm and SDSS DR8 Catalog *Astrophys. J.* **785** 104

[278] Oguri M and Takada M 2011 Combining cluster observables and stacked weak lensing to probe dark energy: self-calibration of systematic uncertainties *Phys. Rev.* D **83** 023008

[279] Hu W and Keeton C R 2002 Three-dimensional mapping of dark matter *Phys. Rev.* D **66** 063506

[280] Marian L, Smith R E and Bernstein G M 2009 The cosmology dependence of weak lensing cluster counts *Astrophys. J.* **698** L33–6

[281] Dietrich J P and Hartlap J 2010 Cosmology with the shear-peak statistics *Mon. Not. R. Astron. Soc.* **402** 1049

[282] Rozo E *et al* 2010 Cosmological constraints from the SDSS maxBCG cluster catalog *Astrophys. J.* **708** 645–60

[283] Mantz A, Allen S W, Rapetti D and Ebeling H 2010 The observed growth of massive galaxy clusters I: statistical methods and cosmological constraints *Mon. Not. R. Astron. Soc.* **406** 1759–72

[284] Tinker J L *et al* 2012 Cosmological constraints from galaxy clustering and the mass-to-number ratio of galaxy clusters *Astrophys. J.* **745** 16

[285] Mantz A B, Allen S W, Morris R G, Rapetti D A, Applegate D E, Kelly P L, von der Linden A and Schmidt R W 2014 Cosmology and astrophysics from relaxed galaxy clusters—II. Cosmological constraints *Mon. Not. R. Astron. Soc.* **440** 2077–98

[286] de Haan T *et al* and SPT Collaboration 2016 Cosmological constraints from galaxy custers in the 2500 square-degree SPT-SZ survey *Astrophys. J.* **832** 95

[287] Schmidt F 2010 Dynamical masses in modified gravity *Phys. Rev.* D **81** 103002

[288] Becker M R and Kravtsov A V 2011 On the accuracy of weak lensing cluster mass reconstructions *Astrophys. J.* **740** 25

[289] Rasia E *et al* 2012 Lensing and x-ray mass estimates of clusters (SIMULATION) *New J. Phys.* **14** 055018

[290] von der Linden A *et al* 2014 Weighing the Giants—I. Weak-lensing masses for 51 massive galaxy clusters: project overview, data analysis methods and cluster images *Mon. Not. R. Astron. Soc.* **439** 2–27

[291] Rykoff E S *et al* and DES Collaboration 2016 The redMaPPer galaxy cluster catalog from DES science verification data *Astrophys. J. Suppl.* **224** 1

[292] Huterer D, Kim A, Krauss L M and Broderick T 2004 Redshift accuracy requirements for future supernova and number count surveys *Astrophys. J.* **615** 595

[293] Lima M and Hu W 2007 Photometric redshift requirements for self-calibration of cluster dark energy studies *Phys. Rev.* D **76** 123013

[294] Levine E S, Schulz A E and White M J 2002 Future galaxy cluster surveys: the effect of theory uncertainty on constraining cosmological parameters *Astrophys. J.* **577** 569–78

[295] Majumdar S and Mohr J J 2004 Self calibration in cluster studies of dark energy: combining the cluster redshift distribution, the power spectrum and mass measurements *Astrophys. J.* **613** 41–50

[296] Lima M and Hu W 2005 Self-calibration of cluster dark energy studies: observable-mass distribution *Phys. Rev.* D **72** 043006

[297] Rozo E, Bartlett J G, Evrard A E and Rykoff E S 2014 Closing the loop: a self-consistent model of optical, x-ray and Sunyaev–Zel'dovich scaling relations for clusters of Galaxies *Mon. Not. R. Astron. Soc.* **438** 78–96

[298] Brainerd T G, Blandford R D and Smail I 1996 Measuring galaxy masses using galaxy–galaxy gravitational lensing *Astrophys. J.* **466** 623

[299] Fischer P *et al* and SDSS Collaboration 2000 Weak lensing with SDSS commissioning data: the Galaxy mass correlation function to 1 h^{-1} Mpc *Astron. J.* **120** 1198–208

[300] Hoekstra H, Yee H K C and Gladders M D 2004 Properties of galaxy dark matter halos from weak lensing *Astrophys. J.* **606** 67–77

[301] Sheldon E S *et al* and SDSS Collaboration 2004 The galaxy—mass correlation function measured from weak lensing in the SDSS *Astron. J.* **127** 2544–64

[302] Mandelbaum R, Seljak U, Kauffmann G, Hirata C M and Brinkmann J 2006 Galaxy halo masses and satellite fractions from galaxy–galaxy lensing in the sdss: stellar mass, luminosity, morphology and environment dependencies *Mon. Not. R. Astron. Soc.* **368** 715

[303] Johnston D E, Sheldon E S, Wechsler R H, Rozo E, Koester B P, Frieman J A, McKay T A, Evrard A E, Becker M R, Annis J and SDSS Collaboration 2007 Cross-correlation weak lensing of SDSS galaxy clusters II: cluster density profiles and the Mass–Richness relation (arXiv:0709.1159)

[304] Choi A, Tyson J A, Morrison C B, Jee M J, Schmidt S J, Margoniner V E and Wittman D M 2012 Galaxy-mass correlations on 10 Mpc scales in the deep lens survey *Astrophys. J.* **759** 101

[305] Velander M *et al* 2014 CFHTLenS: the relation between galaxy dark matter haloes and baryons from weak gravitational lensing *Mon. Not. R. Astron. Soc.* **437** 2111–36

[306] Leauthaud A *et al* 2017 Lensing is low: cosmology, galaxy formation, or new physics? *Mon. Not. R. Astron. Soc.* **467** 3024
[307] Prat J *et al* and DES Collaboration 2017 Dark energy survey year 1 results: galaxy–galaxy lensing (arXiv:1708.01537)
[308] Miralda-Escude J 1991 The correlation function of galaxy ellipticities produced by gravitational lensing *Astrophys. J.* **380**
[309] Wilson G, Kaiser N, Luppino G A and Cowie L L 2001 Galaxy halo masses from galaxy–galaxy lensing *Astrophys. J.* **555** 572–84
[310] Kleinheinrich M *et al* 2006 Weak lensing measurements of dark matter halos of galaxies from COMBO-17 *Astron. Astrophys.* **455** 441–51
[311] Mandelbaum R *et al* 2006 Density profiles of galaxy groups and clusters from SDSS galaxy–galaxy weak lensing *Mon. Not. R. Astron. Soc.* **372** 758–76
[312] Johnston D E *et al* and SDSS Collaboration 2007 Cross-correlation weak lensing of SDSS galaxy clusters II: cluster density profiles and the Mass–Richness relation (arXiv:0709.1159)
[313] Leauthaud A *et al* 2010 A weak lensing study of x-ray groups in the COSMOS survey: form and evolution of the mass-luminosity relation *Astrophys. J.* **709** 97–114
[314] Sheldon E S *et al* and SDSS Collaboration 2009 Cross-correlation Weak Lensing of SDSS Galaxy Clusters III: Mass-to-light Ratios *Astrophys. J.* **703** 2232–48
[315] Hu W and Jain B 2004 Joint galaxy-lensing observables and the dark energy *Phys. Rev.* D **70** 043009
[316] Schmidt F 2008 Weak lensing probes of modified gravity *Phys. Rev.* D **78** 043002
[317] Kochanek C S 1996 Is there a cosmological constant? *Astrophys. J.* **466** 638
[318] Huterer D and Ma C-P 2004 Constraints on the inner cluster mass profile and the power spectrum normalization from strong lensing statistics *Astrophys. J.* **600** L7
[319] Chae K H *et al* 2002 Constraints on cosmological parameters from the analysis of the cosmic lens all sky survey radio—selected gravitational lens statistics *Phys. Rev. Lett.* **89** 151301
[320] Refsdal S 1964 On the possibility of determining Hubble's parameter and the masses of galaxies from the gravitational lens effect *Mon. Not. R. Astron. Soc.* **128** 307
[321] Linder E V 2011 Lensing time delays and cosmological complementarity *Phys. Rev.* D **84** 123529
[322] Suyu S H *et al* 2013 Two accurate time-delay distances from strong lensing: implications for cosmology *Astrophys. J.* **766** 70
[323] Suyu S H, Marshall P J, Auger M W, Hilbert S, Blandford R D, Koopmans L V E, Fassnacht C D and Treu T 2010 Dissecting the gravitational lens B1608+656. II. Precision measurements of the hubble constant, spatial curvature and the dark energy equation of state *Astrophys. J.* **711** 201–21
[324] Linder E V 2004 Strong gravitational lensing and dark energy complementarity *Phys. Rev.* D **70** 043534
[325] Paraficz D and Hjorth J 2009 Gravitational lenses as cosmic rulers: density of dark matter and dark energy from time delays and velocity dispersions *Astron. Astrophys.* **507** L49
[326] Jee I, Komatsu E and Suyu S H 2015 Measuring angular diameter distances of strong gravitational lenses *J. Cosmol. Astropart. Phys.* JCAP11(2015)033
[327] Jee I, Komatsu E, Suyu S H and Huterer D 2016 Time-delay cosmography: increased leverage with angular diameter distances *J. Cosmol. Astropart. Phys.* JCAP04(2016)031
[328] Treu T and Marshall P J 2016 Time delay cosmography *Astron. Astrophys. Rev.* **24** 11
[329] Kaiser N 1987 Clustering in real space and in redshift space *Mon. Not. R. Astron. Soc.* **227** 1–27
[330] Song Y-S and Percival W J 2009 Reconstructing the history of structure formation using Redshift Distortions *J. Cosmol. Astropart. Phys.* JCAP10(2009)004
[331] Percival W J and White M 2009 Testing cosmological structure formation using redshift-space distortions *Mon. Not. R. Astron. Soc.* **393** 297
[332] Linder E V 2008 Redshift distortions as a probe of gravity *Astropart. Phys.* **29** 336–9
[333] de la Torre S *et al* 2013 The VIMOS public extragalactic redshift survey (VIPERS). Galaxy clustering and redshift-space distortions at $z = 0.8$ in the first data release *Astron. Astrophys.* **557** A54
[334] Beutler F *et al* and BOSS Collaboration 2014 The clustering of galaxies in the SDSS-III baryon oscillation spectroscopic survey: testing gravity with redshift-space distortions using the power spectrum multipoles *Mon. Not. R. Astron. Soc.* **443** 1065–89
[335] Johnson A *et al* 2014 The 6dF galaxy velocity survey: cosmological constraints from the velocity power spectrum *Mon. Not. R. Astron. Soc.* **444** 3926
[336] Huterer D, Shafer D, Scolnic D and Schmidt F 2017 Testing ΛCDM at the lowest redshifts with SN Ia and galaxy velocities *J. Cosmol. Astropart. Phys.* JCAP05(2017)015
[337] Turnbull S J, Hudson M J, Feldman H A, Hicken M, Kirshner R P and Watkins R 2012 Cosmic flows in the nearby universe from Type Ia Supernovae *Mon. Not. R. Astron. Soc.* **420** 447–54
[338] Beutler F, Blake C, Colless M, Jones D H, Staveley-Smith L, Poole G B, Campbell L, Parker Q, Saunders W and Watson F 2012 The 6dF galaxy survey: $z \approx 0$ measurement of the growth rate and σ_8 *Mon. Not. R. Astron. Soc.* **423** 3430–44
[339] Blake C *et al* 2013 Galaxy and mass assembly (GAMA): improved cosmic growth measurements using multiple tracers of large-scale structure *Mon. Not. R. Astron. Soc.* **436** 3089
[340] Blake C *et al* 2011 The WiggleZ dark energy survey: the growth rate of cosmic structure since redshift $z = 0.9$ *Mon. Not. R. Astron. Soc.* **415** 2876
[341] Beutler F *et al* and BOSS Collaboration 2016 The clustering of galaxies in the completed SDSS-III baryon oscillation spectroscopic survey: anisotropic galaxy clustering in Fourier-space *Submitted to: Mon. Not. R. Astron. Soc.*
[342] Kaiser N 1989 Theoretical implications of deviations from Hubble flow *Mon. Not. R. Astron. Soc.* **231** 149
[343] Gorski K M, Davis M, Strauss M A, White S D M and Yahil A 1989 Cosmological velocity correlations—observations and model predictions *Astrophys. J.* **344** 1–19
[344] Haugboelle T, Hannestad S, Thomsen B, Fynbo J, Sollerman J and Jha S 2007 The velocity field of the local universe from measurements of Type Ia supernovae *Astrophys. J.* **661** 650–9
[345] Gordon C, Land K and Slosar A 2007 Cosmological constraints from Type Ia supernovae peculiar velocity measurements *Phys. Rev. Lett.* **99** 081301
[346] Ma Y-Z, Gordon C and Feldman H A 2011 The peculiar velocity field: constraining the tilt of the Universe *Phys. Rev.* D **83** 103002
[347] Dai D-C, Kinney W H and Stojkovic D 2011 Measuring the cosmological bulk flow using the peculiar velocities of supernovae *J. Cosmol. Astropart. Phys.* JCAP04(2011)015
[348] Nusser A and Davis M 2011 The cosmological bulk flow: consistency with ΛCDM and $z \approx 0$ constraints on σ_8 and γ *Astrophys. J.* **736** 93
[349] Weyant A, Wood-Vasey M, Wasserman L and Freeman P 2011 An unbiased method of modeling the local peculiar velocity field with Type Ia supernovae *Astrophys. J.* **732** 65

[350] Ma Y-Z and Scott D 2013 Cosmic bulk flows on 50 h^{-1} Mpc scales: a Bayesian hyper-parameter method and multi-shells likelihood analysis *Mon. Not. R. Astron. Soc.* **428** 2017
[351] Rathaus B, Kovetz E D and Itzhaki N 2013 Studying the peculiar velocity bulk flow in a sparse survey of Type-Ia SNe *Mon. Not. R. Astron. Soc.* **431** 3678
[352] Feindt U *et al* 2013 Measuring cosmic bulk flows with Type Ia supernovae from the nearby supernova factory *Astron. Astrophys.* **560** A90
[353] Ma Y-Z and Pan J 2014 An estimation of local bulk flow with the maximum-likelihood method *Mon. Not. R. Astron. Soc.* **437** 1996–2004
[354] Carrick J, Turnbull S J, Lavaux G and Hudson M J 2015 Cosmological parameters from the comparison of peculiar velocities with predictions from the 2M++ density field *Mon. Not. R. Astron. Soc.* **450** 317–32
[355] Riess A G *et al* 2016 A 2.4% determination of the local value of the hubble constant *Astrophys. J.* **826** 56
[356] Bernal J L, Verde L and Riess A G 2016 The trouble with H_0 *J. Cosmol. Astropart. Phys.* JCAP10(2016)019
[357] Hu W 2005 Dark energy probes in light of the CMB *ASP Conf. Ser.* 339 215
[358] Lee J and Park D 2009 Constraining dark energy equation of state with cosmic voids *Astrophys. J.* **696** L10–2
[359] Lavaux G and Wandelt B D 2012 Precision cosmography with stacked voids *Astrophys. J.* **754** 109
[360] Sutter P M, Lavaux G, Wandelt B D and Weinberg D H 2012 A public void catalog from the SDSS DR7 Galaxy Redshift Surveys based on the watershed transform *Astrophys. J.* **761** 44
[361] Nadathur S and Hotchkiss S 2014 A robust public catalogue of voids and superclusters in the SDSS Data Release 7 galaxy surveys *Mon. Not. R. Astron. Soc.* **440** 1248–62
[362] Leclercq F, Jasche J, Sutter P M, Hamaus N and Wandelt B 2015 Dark matter voids in the SDSS galaxy survey *J. Cosmol. Astropart. Phys.* JCAP03(2015)047
[363] Hamaus N, Pisani A, Sutter P M, Lavaux G, Escoffier S, Wandelt B D and Weller J 2016 Constraints on Cosmology and Gravity from the Dynamics of Voids *Phys. Rev. Lett.* **117** 091302
[364] Sutter P M, Lavaux G, Wandelt B D and Weinberg D H 2013 A response to arXiv: 1310.2791: A self-consistent public catalogue of voids and superclusters in the SDSS Data Release 7 galaxy surveys (arXiv:1310.5067)
[365] Jain B and Van Waerbeke L V 2000 Statistics of dark matter halos from gravitational lensing *Astrophys. J.* **530** L1
[366] Hamana T, Takada M and Yoshida N 2004 Searching for massive clusters in weak lensing surveys *Mon. Not. R. Astron. Soc.* **350** 893
[367] Hennawi J F and Spergel D N 2005 Mass selected cluster cosmology. 1: tomography and optimal filtering *Astrophys. J.* **624** 59
[368] Marian L and Bernstein G M 2006 Dark energy constraints from lensing-detected galaxy clusters *Phys. Rev.* D **73** 123525
[369] Dietrich J P and Hartlap J 2010 Cosmology with the shear-peak statistics *Mon. Not. R. Astron. Soc.* **402** 1049
[370] Kratochvil J M, Haiman Z and May M 2010 Probing cosmology with weak lensing peak counts *Phys. Rev.* D **81** 043519
[371] Liu J, Petri A, Haiman Z, Hui L, Kratochvil J M and May M 2015 Cosmology constraints from the weak lensing peak counts and the power spectrum in CFHTLenS data *Phys. Rev.* D **91** 063507
[372] Hamana T, Sakurai J, Koike M and Miller L 2015 Cosmological constraints from Subaru weak lensing cluster counts *Publ. Astron. Soc. Japan* **67** 34
[373] Kacprzak T *et al* and DES Collaboration 2016 Cosmology constraints from shear peak statistics in dark energy survey science verification data *Mon. Not. R. Astron. Soc.* **463** 3653–73
[374] Liu J and Haiman Z 2016 Origin of weak lensing convergence peaks *Phys. Rev.* D **94** 043533
[375] Marian L, Smith R E and Bernstein G M 2010 The impact of correlated projections on weak lensing cluster counts *Astrophys. J.* **709** 286–300
[376] Lin C-A and Kilbinger M 2015 A new model to predict weak-lensing peak counts I. Comparison with *N*-body Simulations *Astron. Astrophys.* **576** A24
[377] Schmidt F and Rozo E 2011 Weak lensing peak finding: estimators, filters and biases *Astrophys. J.* **735** 119
[378] Jimenez R and Loeb A 2002 Constraining cosmological parameters based on relative galaxy ages *Astrophys. J.* **573** 37–42
[379] Stern D, Jimenez R, Verde L, Kamionkowski M and Stanford S A 2010 Cosmic chronometers: constraining the equation of state of dark energy. I: H(z) measurements *J. Cosmol. Astropart. Phys.* JCAP02(2010)008
[380] Moresco M *et al* 2012 Improved constraints on the expansion rate of the Universe up to z 1.1 from the spectroscopic evolution of cosmic chronometers *J. Cosmol. Astropart. Phys.* JCAP08(2012)006
[381] Moresco M, Pozzetti L, Cimatti A, Jimenez R, Maraston C, Verde L, Thomas D, Citro A, Tojeiro R and Wilkinson D 2016 A 6% measurement of the Hubble parameter at $z\sim 0.45$: direct evidence of the epoch of cosmic re-acceleration *J. Cosmol. Astropart. Phys.* JCAP05(2016)014
[382] Schutz B F 1986 Determining the hubble constant from gravitational wave observations *Nature* **323** 310–1
[383] Holz D E and Hughes S A 2005 Using gravitational-wave standard sirens *Astrophys. J.* **629** 15–22
[384] Dalal N, Holz D E, Hughes S A and Jain B 2006 Short GRB and binary black hole standard sirens as a probe of dark energy *Phys. Rev.* D **74** 063006
[385] Cutler C and Holz D E 2009 Ultra-high precision cosmology from gravitational waves *Phys. Rev.* D **80** 104009
[386] Chen H-Y and Holz D E 2016 Finding the one: identifying the host galaxies of gravitational-wave sources (arXiv:1612.01471)
[387] Sandage A 1962 The change of redshift and apparent luminosity of galaxies due to the deceleration of selected expanding universes *Astrophys. J.* **136** 319–33
[388] Linder E V 1997 *First Principles of Cosmology* (Harlow: Addison-Wesley)
[389] Loeb A 1998 Direct measurement of cosmological parameters from the cosmic deceleration of extragalactic objects *Astrophys. J.* **499** L111
[390] Liske J *et al* 2008 Cosmic dynamics in the era of extremely large telescopes *Mon. Not. R. Astron. Soc.* **386** 1192–218
[391] Corasaniti P-S, Huterer D and Melchiorri A 2007 Exploring the dark energy redshift desert with the sandage-loeb test *Phys. Rev.* D **75** 062001
[392] Quercellini C, Amendola L, Balbi A, Cabella P and Quartin M 2012 Real-time cosmology *Phys. Rep.* **521** 95–134
[393] Kim A G, Linder E V, Edelstein J and Erskine D 2015 Giving cosmic redshift drift a whirl *Astropart. Phys.* **62** 195–205
[394] Yu H-R, Zhang T-J and Pen U-L 2014 Method for direct measurement of cosmic acceleration by 21 cm absorption systems *Phys. Rev. Lett.* **113** 041303
[395] Klöckner H-R, Obreschkow D, Martins C, Raccanelli A, Champion D, Roy A L, Lobanov A, Wagner J and Keller R 2015 Real time cosmology—A direct measure of the expansion rate of the Universe with the SKA *PoS* **AASKA14** 027

[396] Daly R A 1994 Cosmology with powerful extended radio sources *Astrophys. J.* **426** 38–50

[397] Daly R A and Guerra E J 2002 Quintessence, cosmology and FRIIb radio galaxies *Astron. J.* **124** 1831

[398] Risaliti G and Lusso E 2015 A hubble diagram for quasars *Astrophys. J.* **815** 33

[399] Schaefer B E 2003 Gamma-ray burst hubble diagram to $z = 4.5$ *Astrophys. J.* **583** L67–70

[400] Amati L *et al* 2002 Intrinsic spectra and energetics of BeppoSAX gamma-ray bursts with known redshifts *Astron. Astrophys.* **390** 81

[401] Amati L 2006 The E(p,i)—E(iso) correlation in grbs: updated observational status, re-analysis and main implications *Mon. Not. R. Astron. Soc.* **372** 233–45

[402] Schaefer B E 2007 The hubble diagram to redshift > 6 from 69 gamma-ray bursts *Astrophys. J.* **660** 16–46

[403] Holz D E and Perlmutter S 2012 The most massive objects in the Universe *Astrophys. J.* **755** L36

[404] Mortonson M J, Hu W and Huterer D 2011 Simultaneous falsification of ΛCDM and quintessence with massive, distant clusters *Phys. Rev.* D **83** 023015

[405] Hotchkiss S 2011 Quantifying the rareness of extreme galaxy clusters *J. Cosmol. Astropart. Phys.* JCAP07(2011)004

Dragan Huterer is a professor of Physics at the University of Michigan.

Daniel L Shafer is a postdoctoral fellow in Physics and Astronomy at Johns Hopkins University.